GEOLOGY OF THE SIERRA MADERA CRYPTOEXPLOSION STRUCTURE, PECOS COUNTY, TEXAS

CONTRIBUTIONS TO ASTROGEOLOGY

Prepared on behalf of the National Aeronautics and Space Administration

GEOLOGICAL SURVEY PROFESSIONAL PAPER 599-H

Geology of the Sierra Madera Cryptoexplosion Structure, Pecos County, Texas

By H. G. WILSHIRE, T. W. OFFIELD, K. A. HOWARD, *and* DAVID CUMMINGS

CONTRIBUTIONS TO ASTROGEOLOGY

GEOLOGICAL SURVEY PROFESSIONAL PAPER 599-H

Prepared on behalf of the National Aeronautics and Space Administration

UNITED STATES GOVERNMENT PRINTING OFFICE, WASHINGTON : 1972

UNITED STATES DEPARTMENT OF THE INTERIOR

ROGERS C. B. MORTON, *Secretary*

GEOLOGICAL SURVEY

V. E. McKelvey, *Director*

Library of Congress catalog-card No. 72-600154

For sale by the Superintendent of Documents, U.S. Government Printing Office, Washington, D.C. 20402
Price: Paper cover—$2, domestic postpaid; $1.75, GPO Bookstore. Stock No. 2401-00238

CONTENTS

ILLUSTRATIONS

[Plates are in pocket]

TABLES

CONTRIBUTIONS TO ASTROGEOLOGY

GEOLOGY OF THE SIERRA MADERA CRYPTOEXPLOSION STRUCTURE, PECOS COUNTY, TEXAS

By H. G. WILSHIRE, T. W. OFFIELD, KEITH A. HOWARD, and DAVID CUMMINGS

ABSTRACT

The Sierra Madera structure is a bowl- or funnel-shaped body, about 8 miles in diameter and 6,000 to 8,000 feet deep, of intensely deformed sedimentary rocks at the southern edge of the Val Verde basin in west Texas. The deformed rocks are Permian and Lower Cretaceous shelf-facies carbonate strata. The structure is composed of three main parts: a central uplift, about 5 miles across, in which the oldest rocks have been raised 4,000 feet above their normal position; a surrounding structural depression, about ½ to 1 mile wide, that is floored mainly by Lower Cretaceous strata; and a concentric structurally high rim, about half a mile wide, in which Lower Cretaceous rocks are locally folded and cut by concentric normal faults downthrown toward the center.

The intensity of folding and faulting increases inward from the flanks of the central uplift toward a central zone, about a mile in diameter, where dips and fold plunges are near vertical or overturned. Individual beds are repeated by folding and faulting, so that their total strike length is greater than the length of the perimeter on which they lie, indicating both inward and upward movement of the strata forming the uplift. This movement pattern is substantiated by a thickened section in the center where only 1,200 feet of the oldest strata with generally steep dips fill an area at least a mile wide. Drill data show that this thickening is not the result of domical arching of the oldest beds but is instead, caused by repetition of beds resulting from centripetal movement.

The structural depression probably resulted from tectonic thinning accompanying the inward movement of rocks to form the central uplift. Folding and uplift in the outer rim may have been produced by outward-directed compression early in the deformational event.

Monolithologic and mixed breccias, shatter cones, and certain types of internal structures of minerals at Sierra Madera are ascribed to shock deformation. Monolithologic breccias, composed of shattered but unmixed rocks, are abundant on the central uplift. Generally, they show few signs of shock deformation, but there are indications that some shatter cones formed concurrently. When beds containing shatter cones are restored to horizontal, the cones point inward and upward above the center of the structure. Mixed breccias form intrusive bodies in which fragments from beds as much as 1,700 feet apart occur together. Quartz grains in the mixed breccias have multiple planar elements and cleavages, dominantly parallel to {0001}, {10$\bar{1}$3}, {10$\bar{1}$2}, {10$\bar{1}$1}, and {10$\bar{1}$0}, and abnormally low refractive indices that indicate peak pressures above 200 kb (kilobars). Planar elements in quartz from rocks still in place near the center of the structure record pressures above 100 kb, and those in quartz from rocks on the flanks of the uplift record pressures near 50 kb.

The symmetry of restored shatter-cone orientations suggests that the cones were formed by a shock wave of generally hemispherical form. As the shock wave traveled downward and outward from the central focus, shock intensity progressively decreased. Only the surface impact of an extraterrestrial body could have produced such a shock wave. This interpretation is supported by the uniqueness of Sierra Madera in an otherwise normal geologic environment, its lack of relation to any regional or local structure, and the geometry of the central uplift, which could not have been produced by a deep subsurface explosive event.

Although the mechanics of formation of the central uplift are still not completely understood, its structure is similar to uplifts in craters formed by surface detonation of TNT (trinitrotoluene) in Canadian cratering experiments. Analogy with experimental craters and with other cryptoexplosion structures indicates that the uplift at Sierra Madera protruded into a crater, since destroyed by erosion, that was about 8 miles in diameter. Inasmuch as the rocks forming such uplifts are derived from below the crater floors, analogous lunar craters potentially offer samples of lunar crust uplifted from distances below the crater floor on the order of one-tenth the crater diameter.

INTRODUCTION

Sierra Madera (wooded hills) is a small group of hills about 3 miles in diameter that rise 600 feet above the plains between the Glass Mountains and Fort Stockton in west Texas (fig. 1). The hills are encircled at a distance of about 2 miles by a ring of hills that rises only slightly above the general level of the plains. Between these two features is an annular depression largely covered by alluvium. Six Shooter Draw, an intermittent stream, breaches the outer ring of hills on the southwest and northeast sides and follows the annular depression along a crescent-shaped path around the west side of Sierra Madera. The Sierra Madera structure, about 8 miles in diameter, includes the central hills from which it takes its name, the annular depression, and the outlying ring of low hills.

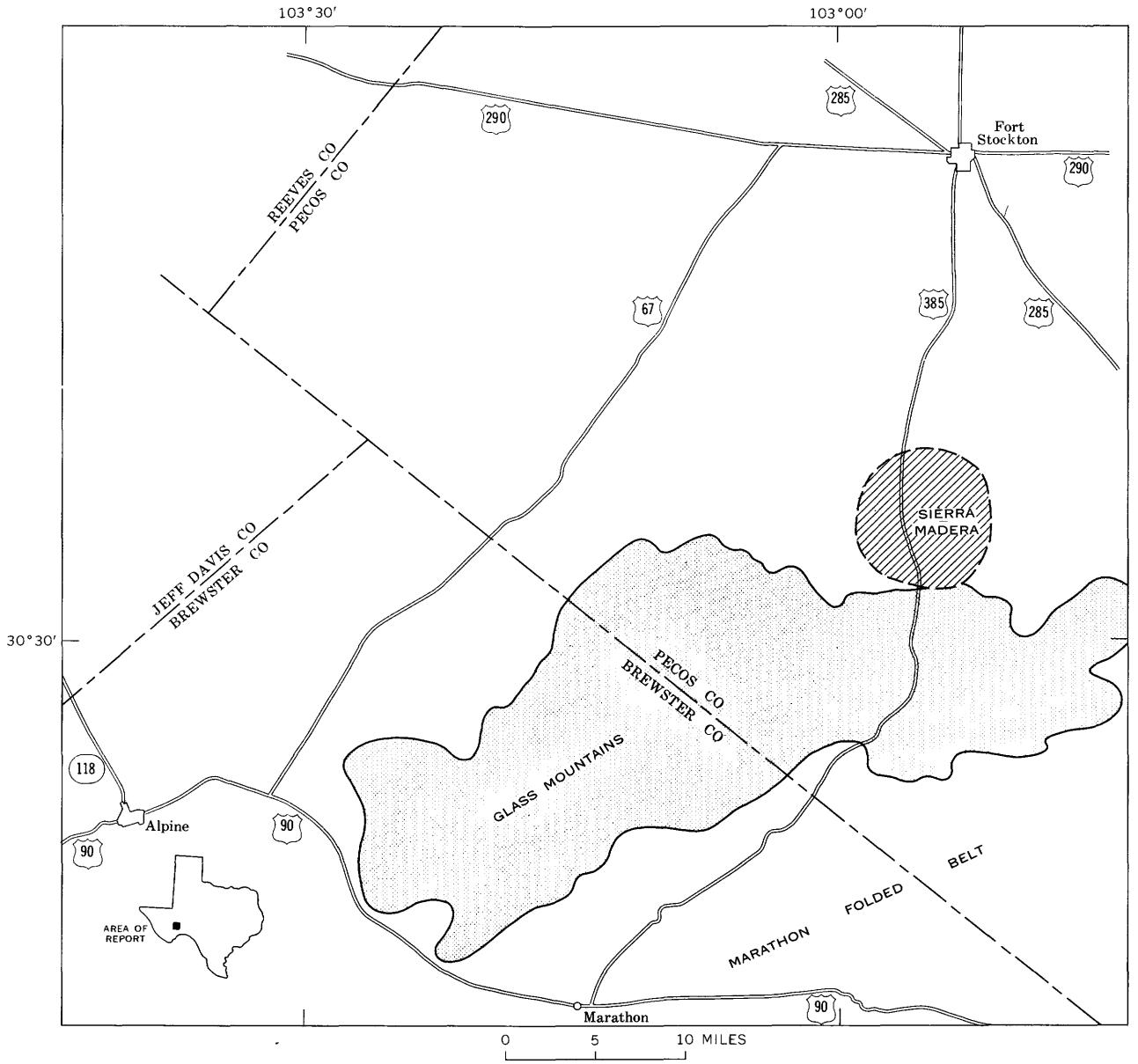

FIGURE 1.—Index map of Pecos and adjacent counties, west Texas, showing location of the Sierra Madera structure, the Glass Mountains, and part of the Marathon folded belt.

The Sierra Madera structure is one of a class characterized by roughly circular areas enclosing a central zone of uplifted and intensely deformed rocks surrounded by a ring of subsided rocks with or without an outlying zone of concentric folds. Bucher (1936) denoted these by the name "cryptovolcanic," originally used for the Steinheim structure (Branco and Fraas, 1905). Subsequent work has shown that such structures are also characterized by the presence of shatter cones (Dietz, 1968) and unusual types of mineral deformation (Short, 1966a), which support the idea, dating back to the work of Branco and Fraas (1905), that these structures formed by explosive release of energy. Whether the source of the energy was terrestrial or extraterrestrial has been the subject of lively controversy for more than three decades (Bucher, 1936; Boon and Albritton, 1936). To describe these structures without bias toward terrestrial or extraterrestrial origin, Dietz (1946) introduced the term "cryptoexplosion structure," to which Bucher (1963) later subscribed.

The current investigation of Sierra Madera was begun in 1960 by E. M. Shoemaker to provide detailed information on the geology of this well-exposed structure. The main impetus of the study was to obtain information on possible terrestrial analogs of lunar structures.

PREVIOUS WORK

The first geologic map of Sierra Madera was made by King (1930) as part of a regional study of the Glass Mountains. He recognized the unusual character of the structure (p. 123), and his comparison (p. 125) of Sierra Madera with the Vredefort ring of South Africa led Boon and Albritton (1937) to their challenging suggestion that these two structures as well as others like them are of meteorite impact origin. King (p. 124) further demonstrated the domical uplift of the center and noted evidence for severe radial compression of the uplifted rocks, both of which are confirmed by our work. His suggestion (p. 125) that igneous intrusion may have played a role in formation of the structure was subsequently disproved by holes drilled for oil and gas.

Shatter cones were discovered at Sierra Madera in 1959 (Eggleton and Shoemaker, 1961, p. 151), and were later studied in detail by Howard and Offield (1968). Shoemaker and Eggleton (1964) found, contrary to King's interpretation, that Lower Cretaceous rocks at Sierra Madera are as severely deformed as adjacent Permian rocks and concluded that the structure was formed by a single episode of deformation some time after deposition of Lower Cretaceous rocks. Eggleton and Shoemaker (1961) described the breccias in the central uplift of Sierra Madera as a cup-shaped mass resembling the breccia zones under Meteor Crater (Arizona) and the nuclear crater Teapot Ess (Nevada Test Site).

Lowman (1965) made a reconnaissance magnetic survey that revealed a magnetic high under the southeast part of the central uplift and tentatively concluded that Sierra Madera was formed by a syenite intrusion. Van Lopik and Geyer (1963) suggested that the aforementioned anomaly may be caused by meteoritic material, but the data are not yet adequate to distinguish among the possible causes of the anomaly.

In most of the foregoing studies, the structure was thought to be confined to the topographic feature of Sierra Madera, 3 miles in diameter, but it is now known to include two other structural elements—a concentric structural depression and a peripheral ring of folds and faults.

ACKNOWLEDGMENTS

This work was done on behalf of the National Aeronautics and Space Administration under contract R–66. We are indebted to R. P. Bryson and V. M. Wilmarth (NASA) for their interest and encouragement. P. B. King, D. J. Milton, D. J. Roddy, O. B. James, and E. C. T. Chao, U.S. Geological Survey, critically read the manuscript and considerably improved this final version by their suggestions. Discussion of the problems at various stages of the project with D. J. Milton, U.S. Geological Survey, was of great benefit to us. We are especially indebted to Addison Young, J. L. Williams, and C. J. Perusek, Phillips Petroleum Co.; G. L. Evans, Louisiana Land and Exploration Co.; V. O. Cook and Y. B. Newsom, Gulf Oil Corp.; and J. K. Somerville, Southern Natural Gas Co.; for their interest and cooperation. The cooperation of E. M. Shoemaker, California Institute of Technology, and R. E. Eggleton and D. P. Elston, U.S. Geological Survey, is gratefully acknowledged. Access to Sierra Madera and assistance in many other ways were graciously rendered by Mr. Peller Matthews, Elsinore Ranch.

STRATIGRAPHY

Sierra Madera is underlain by a sequence of Cambrian to Lower Cretaceous sedimentary rocks about 18,000 feet thick (fig. 2). They presumably overlie Precambrian crystalline rocks, as granite with an age of 900 million years was penetrated by wells about 23 miles east of Sierra Madera (Young, 1960, p. 89), and silicic plutonic rocks were penetrated on the Fort Stockton high to the north (Flawn, 1956). The pre-Permian Paleozoic strata, mainly carbonate and fine-grained clastic rocks, were deformed in Late Pennsylvanian and very early Permian time during the formation of the Val Verde trough. Sierra Madera is situated on the southern edge of the trough (fig. 3; Young, 1960; Oriel and others, 1967). The 7,000 to 12,000 feet of clastic sedimentary rocks of the Lower Permian Wolfcamp Series (fig. 2) near Sierra Madera were deposited in the Val Verde trough, which, in Wolfcamp time, was continuous with the Delaware basin (fig. 3; Vertrees and others, 1959). Later in Wolfcamp time, the Sierra Madera site became part of a shelf on which carbonate rocks formed. The Hess Formation (fig. 2) is transitional between basin and shelf environments and is composed of interbedded clastic and carbonate rocks. Thin, shallow-water, clastic sedimentary rocks of Triassic age unconformably overlie Permian strata near Sierra Madera but probably do not occur at Sierra Madera. Permian rocks at Sierra Madera are unconformably overlain by a conformable sequence of Lower Cretaceous rocks—the Trinity, Fredericksburg, and Washita Groups—deposited during an extensive transgression of the sea from the Gulf region (Oriel and others, 1967). Cretaceous rocks overlap progressively older Permian rocks southward in the Glass Mountains, a fact indicating pre-Cretaceous tilting of the Glass Mountains Permian sequence (King, 1930, p. 127). Lower Cretaceous and older rocks are partly covered by thin unconsolidated Quaternary deposits.

Rocks exposed at Sierra Madera range in age from Early Permian to Early Cretaceous (Comanche Series).

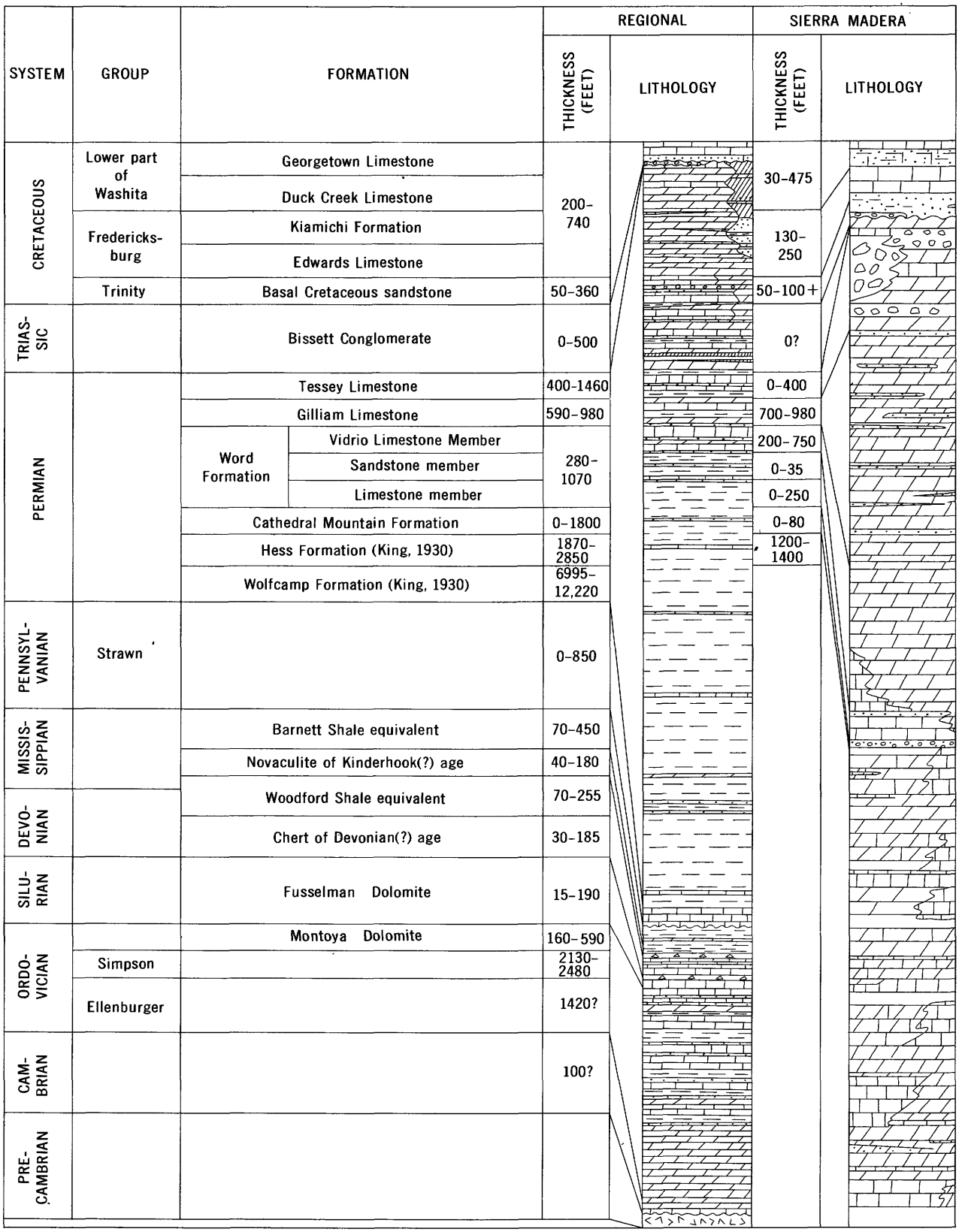

FIGURE 2.—Generalized stratigraphic column of Precambrian to Lower Cretaceous rocks at Sierra Madera (left column) and detailed stratigraphic column of rocks exposed at Sierra Madera (right column).

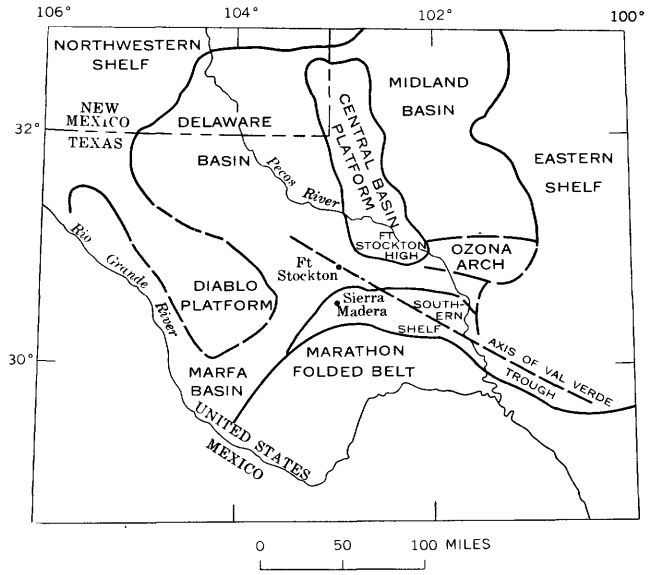

FIGURE 3.—Index map showing the location of Sierra Madera with respect to Permian basins and pre-Permian structures in west Texas and southeastern New Mexico (from Oriel and others, 1967, fig. 7).

The Permian sequence at Sierra Madera is nearly identical with that in the nearby eastern part of the Glass Mountains, and the same stratigraphic units are recognizable (King, 1930). King did not separate the Tessey Limestone, Gilliam Limestone, and Vidrio Limestone Member of the Word Formation at Sierra Madera, but these units were mapped for this report. Formations older than upper Wolfcamp apparently are not deformed as part of the Sierra Madera structure and are only briefly described below.

PRE-PERMIAN SEDIMENTARY ROCKS

Generalized lithologies of pre-Permian sedimentary rocks in the vicinity of Sierra Madera are shown in figure 2. None of the wells that supplied the data for figure 2 penetrated the full thickness of sedimentary rocks, but six bottomed in rocks of the Lower Ordovician Ellenburger Group, not far above the Precambrian rocks. The section between Precambrian crystalline rocks and the Lower Permian Wolfcamp is about 5,000 feet thick. The rocks were deposited in a shallow marine environment. They consist mainly of limestone and dolomite near the base and grade upward to a sequence with a higher proportion of fine-grained clastic material and some chert. All systems from Cambrian to Pennsylvanian are represented, although Pennsylvanian strata are locally missing over a structural high below the southwestern edge of Sierra Madera. (See fig. 6.) The total thickness of this part of the section increases slightly from south to north (table 1), but no significant facies or thickness changes occur in the study area.

TABLE 1.—*Thickness variations, in feet, in the pre-Triassic, post-Ellenburger section from south to north across Sierra Madera*

	South [1]	Hunt 51	North [2]
Tessey Limestone	235	220	1,190
Gilliam Limestone	745	580	
Word Formation: [3]			2,880
Vidrio Limestone Member	385	750	
Limestone Member	115	300	
Hess Formation	2,475	2,850	2,200
Wolfcamp Series exclusive of Hess Formation	7,835	9,110	10,215
Pennsylvanian System	70	380	470
Barnett Shale equivalent	145	450	285
Pre-Barnett, post-Woodford Mississippian System	70	180	
Woodford Shale equivalent	160	160	160
Pre-Woodford Devonian System	55	70	175
Fusselman Dolomite	160	140	50
Montoya Dolomite	450	150	510
Simpson Group	2,365	---	2,290

[1] Averages of data from Hunt Fulk 1, Elsinore 48, 52, 53, 57.
[2] Averages of data from Vacuum Elsinore 1, Phillips Alamo 1, Sinclair-Phillips Montgomery 1.
[3] The sandstone member of the Word Formation was not identified in drill cuttings.

PERMIAN SYSTEM

WOLFCAMP FORMATION (KING, 1930)

The Val Verde trough, which had formed during Wolfcamp time, deepened in Early Permian time, and a thick body of Lower Permian basin-facies clastic sediments was deposited near the site of Sierra Madera. These rocks, 7,000 to 12,000 feet thick, are a monotonous sequence of black shales interbedded with fine-grained sandstone and some clastic(?) limestone and dolomite. These rocks make up the Wolfcamp Formation as used by King (1930). The upper few hundred feet generally contains a higher proportion of limestone and dolomite, which grade into the overlying Hess Formation. There is no lithologic basis for subdividing the Wolfcamp Series, but a paleontologic distinction between upper and lower parts is useful where the data are available. (See fig. 6.)

The Wolfcamp thickens (table 1) from 7,000 feet at the south edge of Sierra Madera to 12,000 feet northeast of it, near the axis of the Val Verde trough (pl. 1, Sinclair-Phillips Montgomery 1; fig. 3).

HESS FORMATION (KING, 1930)

The Hess Formation, as used by King (1930), ranges in thickness from about 2,400 feet at the southern edge of Sierra Madera (pl. 1, Hunt Elsinore 53) to 2,800 feet at the northern edge (table 1; pl. 1, Hunt Elsinore 51) and is transitional between the Wolfcamp basin-facies and younger shelf-facies rocks. The Hess Formation comprises interbedded shale, fine-grained sandstone, dolomite, limestone, and marl. The section shows a general upward increase in carbonate at the expense of sandstone and shale and in dolomite at the expense of limestone. The only marker within the Hess that can be correlated between Sierra Madera and the Glass Mountains consists of varicolored marly beds occurring near the base of the sequence exposed at

Sierra Madera (pls. 2, 3) and about 950 feet below the upper contact in the Glass Mountains. Thin anhydrite beds near the middle of the Hess Formation were penetrated by holes drilled on Sierra Madera, but they are not present in the Glass Mountains. The anhydrite beds are not exposed at Sierra Madera, so that the thickness of Hess strata at the surface probably does not exceed 1,200 to 1,400 feet.

The varicolored marly beds consist of light-gray dolomitic marl interbedded with laminated yellow siltstone and several conspicuous beds of pink medium-grained silty dolomite. Rocks immediately above and below the marly beds are light-gray to brown, finely crystalline, locally cherty dolomite with some thin interbedded finely crystalline limestones. The limestone beds contain fusulinids, brachiopods, and bryozoans; fusulinids in at least one bed have distinctive light halos. Dolomites of the Hess are sparsely fossiliferous (mainly scattered silicified crinoid stems and local concentrations of gastropods). Many dolomite beds have open ellipsoidal to equidimensional cavities about half an inch in diameter. The upper 900 feet of Hess strata exposed at Sierra Madera is composed mainly of thin- to thick-bedded, light-gray to dark brownish gray, finely to coarsely crystalline dolomite, calcareous dolomite, and limestone; rapid lateral changes from one rock type to another are characteristic. Some of the limestones contain abundant fossils, especially fusulinids, but others, mainly massive, medium- to coarse-grained limestones, are barren of fossils. Thin beds of light-gray marly dolomite are interspersed in various parts of the upper 900 feet of exposed strata. A thin, discontinuous bed of dolomite containing quartz granules occurs about 100 feet below the top of the formation on the north side of the structure. The uppermost 50 feet of the formation on the north, east, and south sides contains several beds of light-gray marl and marly dolomite and, in places, a distinctive bed of porous, white, marly dolomite. Notes on the petrography of representative lithologies and fusulinid identifications are given in table 2.

The principal northward (basinward) change (pl. 1,

TABLE 2.—*Petrography and paleontology of rocks exposed at Sierra Madera*

[Units arranged from youngest to oldest. Limestones classified according to Folk (1959, 1962), sandstones according to Williams, Turner, and Gilbert (1954). Fusulinids identified by C. A. Ross, Western Washington State College]

Georgetown, Duck Creek, Kiamichi, and Edwards Formations.	Biomicrite, pelmicrite, and microsparite most abundant; local fine to very coarse, sandy calcirudite. Fossils common, not identified.
Basal Cretaceous sandstone	Fine- to coarse-grained quartz arenite with finely to coarsely crystalline calcite cement, locally with microcrystalline quartz cement; quartz has bimodal size distribution with large subrounded to well-rounded grains and small angular to subangular grains; zoned and weak to moderate undulose extinction fairly common; most grains have fluid inclusions, many in planar concentrations; poorly developed cleavages uncommon; a few grains have one to three sets of thin planar discontinuities. Minor detrital constituents include micrite, chert, tourmaline, rutile, and monazite.
Tessey Limestone	Finely to very finely crystalline dolomite and pellet dolomite; variable quantities of sparry calcite, minor detrital quartz and muscovite. Some interbedded pelmicrite. Dolomites commonly brecciated with clasts in aphanocrystalline groundmass. Fossils fragmental and rare, not identified.
Gilliam Limestone	Finely to very finely crystalline dolomite and pellet dolomite, and fine to very fine grained quartz arenite with very finely to finely crystalline carbonate cement. Sandstones moderately to well sorted, quartz angular to subangular; planar concentrations of fluid inclusions common in quartz; undulose extinction uncommon; cleavage and planar discontinuities rare. Common accessories in sandstones are chert, muscovite, microcline, plagioclase, tourmaline, rutile, zircon, and opaque minerals. Fusulinids and gastropods rare, poorly preserved, not identified.
Word Formation	Vidrio Limestone Member; finely to medium-crystalline dolomite, local dolomitized microsparite, biomicrudite, pelmicrite(?). *Parafusulina sellardsi.* Sandstone Member; finely- to coarse-grained quartz arenite with finely to coarsely crystalline carbonate cement, and sandy finely to medium-crystalline dolomite. Quartz moderately sorted, tendency to bimodal size distribution, subangular to subrounded; undulose extinction uncommon; planar concentrations of fluid inclusions common; cleavage and one to three sets of planar discontinuities uncommon. Minor detrital constituents include chert, biomicrite, micrite, and opaque minerals. Limestone Member; dolomitized biomicrudite, biomicrosparite, microsparite, biosparrudite. *Parafusulina deliciasensis, P. wildei, P. sullivanensis.*
Cathedral Mountain Formation	Conglomerate and fine to very coarse grained quartz arenite with finely to coarsely crystalline carbonate cement. Conglomerate pebbles mainly chert and quartzite. Quartz moderately to poorly sorted, subangular to subrounded; undulose extinction uncommon; planar concentrations of fluid inclusions moderately common; cleavage poorly developed, moderately common; planar structures uncommon but form one to three sets where present, except in quartzite grains where one to five sets of such structures are common.
Hess Formation (King, 1930)	Variously dolomitized microsparite, biomicrorudite, biosparrudite, and finely to coarsely crystalline dolomite. *Schubertella melonica, Parafusulina durhami, P. spissisepta, P. brooksensis, P. splendens, Schwagerina hessensis, P. vidriensis.*

Phillips Alamo 1) in lithology of the Hess Formation is a large increase in proportion of shale and fine-grained sandstone in the upper part. The average thickness of the formation (table 1) is about 300 feet less to the north and east of Sierra Madera.

CATHEDRAL MOUNTAIN FORMATION

The Hess Formation is overlain by a thin sequence of calcareous chert conglomerate, very coarse grained calcareous quartz and chert sandstone, and thin sandy dolomite beds (fig. 2; table 2). These rocks were designated the Leonard Formation by King (1930) and, in the Glass Mountains, were later divided into the Hess, Skinner Ranch, Cathedral Mountain, and Road Canyon Formations by Cooper and Grant (1964, 1966). The formation thins rapidly from the Glass Mountains toward Sierra Madera, and at Sierra Madera it is from 0 to about 80 feet thick. Along the northern side of Sierra Madera the Cathedral Mountain Formation is represented by only a few stringers of chert and quartz pebbles in dolomite and probably disappears altogether a little beyond the northernmost exposures. Cuttings of the conglomerate were not recovered from any of the holes drilled near Sierra Madera.

WORD FORMATION

The Word Formation near Sierra Madera is a shelf-facies deposit of limestone and dolomite that ranges from about 360 to 1,000 feet in thickness. It is here subdivided into three members (fig. 2): informal limestone and sandstone members and the Vidrio Limestone Member (King, 1942). The lowest member, 0 to 250 feet thick, is thick- to thin-bedded, locally platy limestone that is generally richly fossiliferous and contains some interbedded finely crystalline dolomite (table 2). The limestone member is overlain by coarse-grained sandstone composed of angular quartz granules and silicified crinoid segments, or by siltstone and fine-grained sandstone, 0 to 35 feet thick. The sandstone grades laterally to sandy dolomite (table 2), and in places massive dolomite, included as part of the sandstone member, intervenes between the sandstone and underlying limestone member. The uppermost member, the Vidrio, 200 to 750 feet thick, is very thick bedded to massive, gray to dark-brown dolomite. Numerous small disk-shaped cavities elongate parallel to bedding characterize its lower part. Chert is common in the upper half and also near the base; fossils are very rare. Owing to lateral changes in the Word at Sierra Madera (table 2), on the east side the Vidrio Limestone Member includes light-gray, finely crystalline to coarse bioclastic limestone between the sandstone member and dolomite, whereas in other places the sandstone member is missing and the lower limestone member is replaced by dolomite of the Vidrio Limestone Member, which directly overlies the Cathedral Mountain Formation (fig. 2).

All three members of the Word Formation at Sierra Madera occur in the nearby Glass Mountains, but the formation thickens northward beneath the surface (table 1) and changes to interbedded shale, sandstone, limestone, and dolomite (pl. 1, Phillips Alamo 1, Vacuum Elsinore 1).

GILLIAM LIMESTONE

The Gilliam Limestone, about 700 to 950 feet thick at Sierra Madera, is bedded dolomite with variable amounts of very fine and fine-grained sandstone. Dolomite beds are 1 inch to about 3 feet thick; sandstone beds, a few inches to about 6 feet thick. The formation grades downward, with increasing thickness of beds, into the Vidrio Limestone Member. The top is generally marked by a thin sandstone bed. Gray facies and red or brown facies were recognized during fieldwork but are not shown on the map because they do not maintain constant stratigraphic positions. However, one major body of red or brown beds appears to separate upper and lower gray beds to create a threefold subdivision of the formation. This subdivision was used in the structural interpretation.

Dolomite of the gray facies is generally thin bedded and laminated, although some massive beds occur near the gradational contact with the Vidrio Limestone Member. The gray dolomite is mostly very finely to finely crystalline and lacks detrital constituents. The red or brown dolomite is thin bedded and very finely to finely crystalline, and it contains some detrital constituents (table 2). Thin, discontinuous lenticular beds of yellow-brown, very fine to fine-grained sandstone occur irregularly throughout the formation but are more abundant in the red or brown facies than in the gray facies except at the northeast corner of the central uplift (pl. 3).

In drill holes a short distance north of Sierra Madera (pl. 1, Hunt Elsinore 16, 26) the Gilliam Limestone is mainly fine- to medium-grained sandstone (Yates equivalent; Natl. Research Council, 1960) composed of well-rounded quartz grains and chert, in contrast to the dominant dolomite of the exposed section. Farther north (pl. 1, Vacuum Elsinore 1, Phillips Alamo 1), the Gilliam thickens and grades upward into interbedded evaporites and fine-grained clastic rocks (Yates and Tansill equivalents; Natl. Research Council, 1960).

TESSEY LIMESTONE

The Tessey Limestone, from 0 to about 400 feet thick, ranges from thin-bedded, gray, brown, and reddish-brown dolomite to block breccia composed of angular fragments of laminated dolomite a few inches across

in a dolomite matrix, to extremely coarse breccia of randomly oriented dolomite or light-gray limestone blocks several tens of feet long. The very coarse breccia also occurs in the Glass Mountains and at Sierra Madera appears to be localized along the eastern side, where it lies between brecciated and unbrecciated thin-bedded dolomite with rare, thin, sandy dolomite beds (table 2). Elsewhere, the formation is mostly block breccia with small clasts. Massive limestone as much as 100 feet thick is locally present. Fossils are extremely rare in both the dolomite and limestone.

Gradations from undisturbed laminated dolomite to randomly oriented fragments of laminated dolomite in the Glass Mountains indicate that the finer grained block breccia was reworked by currents shortly after it had solidified. The very coarse breccias are presumably reef-related deposits. The wide distribution of Tessey breccias indicates that such breccias are unrelated to the Sierra Madera structure.

The Tessey Limestone changes rapidly northward (pl. 1, Hunt Elsinore 16, 26; Vacuum Elsinore 1; Phillips Alamo 1) to a dominantly saline sequence equivalent to the Salado and Rustler Formations (Natl. Research Council, 1960).

TRIASSIC SYSTEM

BISSETT CONGLOMERMATE

A thin conglomerate composed of chert, quartz, limestone, and dolomite pebbles locally overlying the Tessey at Sierra Madera was tentatively identified by Shoemaker and Eggleton (1964) as the Triassic Bissett Conglomerate. Similar conglomerates occur at several horizons in the overlying basal Cretaceous sandstone, and all may be of Cretaceous age. It might be that the lowest conglomerate, averaging less than a foot thick, is Triassic but was included by us with the basal Cretaceous sandstone at Sierra Madera. Both the Tessey and Bissett change northward to interbedded evaporites and fine-grained clastic rocks.

CRETACEOUS SYSTEM

SANDSTONE

A sandstone (the basal Cretaceous sandstone of Adkins, 1927, p. 31–37; Basement sands of King, 1930, p. 93) at Sierra Madera occurs at the base of the Cretaceous System where it unconformably overlies Permian strata. It is composed of about 50 to 100 feet of gray to reddish-brown fine- to coarse-grained quartz sandstone (table 2) with some interbedded chert, quartz, and carbonate pebble conglomerate, and that contains varicolored silty and shaley lenses. Crossbeds, current ripple marks, rain prints, and flow casts are common. The local absence and extreme thickness variations of the sandstone (pl. 3) on the central uplift are probably the result of the deformation rather than nondeposition or local basin thickening. The distribution of the sandstone is described in detail in a following section (p. H13). The sandstone is cemented by quartz rather than the usual calcite in several roughly equidimensional zones as much as 300 feet across. Silicified pods such as these also occur in the Glass Mountains. Fossil wood fragments are locally abundant in the sandstone at Sierra Madera and were possibly derived from the charophyte that provided spores found in the sandstone near Fort Stockton (Groves, 1925).

FREDERICKSBURG GROUP AND LOWER PART OF WASHITA GROUP

The Fredericksburg and Washita Groups were not mapped individually because of poor exposures of marker beds and lack of paleontologic control. Most of these strata at Sierra Madera, however, belong to the Edwards Limestone of the Fredericksburg Group. The overlying Kiamichi Formation, also in the Fredericksburg Group, occurs only along the northern edge of the map area (pl. 2) but may be present in parts of the ring depression where the thickness of Cretaceous rocks exceeds 250 to 300 feet. The local occurrence (pl. 1, Hunt Elsinore 32, 37, 40) of as much as 740 feet of post-Trinity rocks in apparently little deformed areas indicates that the Duck Creek and Georgetown Limestones, in the lower part of the Washita Group, are also present in the eastern rim zone of Sierra Madera.

The Edwards Limestone, estimated to be between 130 and 200 feet thick, is platy to massive, fine- to coarse-grained, gray to light-brown limestone. In places, on the southeast side of the structure, it includes thin, finely laminated, orange to yellow-brown marl beds, commonly with small-scale internal folds and faults. Limestone beds locally contain irregular, rounded chert nodules and silicified fossils. The base of the formation on the southeastern side of Sierra Madera is locally a limestone breccia, possibly of deformational origin, with scattered broken chert fragments. A conspicuous coquina of silicified fossils lies near the base of the formation on the southeastern side. The top of the formation on the northern rim of Sierra Madera is a brown coarsely crystalline limestone.

The Kiamichi Formation, about 50 feet thick, is interbedded gray and light-brown, shaly or flaggy marl with some thin argillaceous limestone beds. The Kiamichi is overlain by the Duck Creek and Georgetown limestones, which are interbedded platy and massive, fine- to medium-grained limestones, the lower beds of which contain abundant ammonites (*Pervinquieria*). Drill holes Hunt Elsinore 32, 37, and 40 (pl. 1) penetrated as much as 445 feet of the Georgetown Limestone.

QUATERNARY SYSTEM

SURFICIAL DEPOSITS

Alluvium, perhaps over 50 feet thick in the depression surrounding the central uplift of Sierra Madera, consists generally of unsorted to poorly sorted angular to subrounded dolomite, limestone, chert, and sandstone fragments from boulder to silt size. Surficial calcrete is common. A few pebbles of volcanic rocks found on the east side of Sierra Madera as well as on the tops of mesas between Sierra Madera and Fort Stockton were probably derived from Tertiary intrusive or flow rocks (since eroded) in the nearby Glass Mountains. Terraces on the alluvial fill of stream channels on the uplift are common, and locally as many as three terrace levels are present along short segments of the same channel. Colluvium that mantles large areas on the uplift or that obscures important bedrock relationships was also mapped but is not separated from alluvium on the maps.

STRUCTURE

The Sierra Madera structure consists of (1) a central uplift (fig. 4) about 5 miles in diameter in which the oldest Permian rocks are raised about 4,000 feet above their normal position, (2) a surrounding alluviated structural depression about ½ to 1 mile wide that is floored mainly by Lower Cretaceous rocks, and (3) an outer, structurally high rim about half a mile wide of faulted and folded Upper Permian and Lower Cretaceous strata (pl. 2). Each of these zones is prominently expressed in the topography except on the outer rim at the south and southeast sides. Outside the structure, regional joints are unrelated to the circular form (fig. 5); some joints (northwest and north-northwest strikes) cut mixed breccia within the structure and so postdate it. High-altitude photographs show a nearly complete circular form that is apparently, along the south and southeast, marked by concentric drainage. However, no deformation was found along the concentric drainage channels, so that they are apparently controlled by joints that have no fault offsets. Hence, the limits of the structure are set by the mapped limits of deformation, although future mapping with finer subdivision of Lower Cretaceous strata may show that mild deformation extends beyond the presently recognized boundaries.

FIGURE 4.—View west-northwest from the outer rim of Sierra Madera showing the central uplift across the alluviated structural depression in the middle ground. Photograph, courtesy of Jeanette L. Gillette, San Angelo Standard-Times.

Deep holes drilled for oil and gas (pl. 1) show that the intense deformation observed at the surface dies out rapidly at depth and probably disappears in Upper Wolfcamp strata between 6,000 and 8,000 feet below the surface (fig. 6).

Rocks of the central uplift, especially the Permian rocks, but also locally the Lower Cretaceous strata, are pervasively brecciated. The most common type of breccia (fig. 18) consists of thoroughly shattered rock in which fragments are generally so little displaced that thin beds maintain their continuity. (See fig. 17.) A second type of breccia, occurring in generally cross-cutting bodies, contains a mixture of fragments of different lithologies. Examination of cuttings from the Phillips Elsinore 1 well drilled on the center of the structure (pls. 2, 3; Eggleton and Shoemaker, 1961) suggests that both types of breccia become less common downward and are absent about 3,000 feet below the surface.

The gross structure, then, is represented by a bowl-shaped body approximately 8 miles in diameter and 6,000 to 8,000 feet deep, the central part of which has a high structural relief near the present ground surface, with intensely shattered beds that are tightly folded and cut by numerous faults. The intensity of deformation and brecciation decreases outward and downward from this area.

RIM ZONE

The outer rim of the structure consists of faulted and locally folded Upper Permian and Lower Cretaceous strata. There appears to be little or no structural displacement of Cretaceous rocks immediately outside the bounding ring faults at the southwest and south edges of the structure, but Cretaceous strata in the same position relative to circumferential faults along the north and east sides are as much as 100 feet, and perhaps more, above their normal regional level. Both the faults and the fold axes are generally concentric about the central uplift (pl. 2). Folds are best developed from the northeast part of the rim around the east to the southeast corner. Fold axes have a generally low plunge, and limbs generally dip less than 45°. Dips are as steep as 90° in places but do not persist more than a few tens

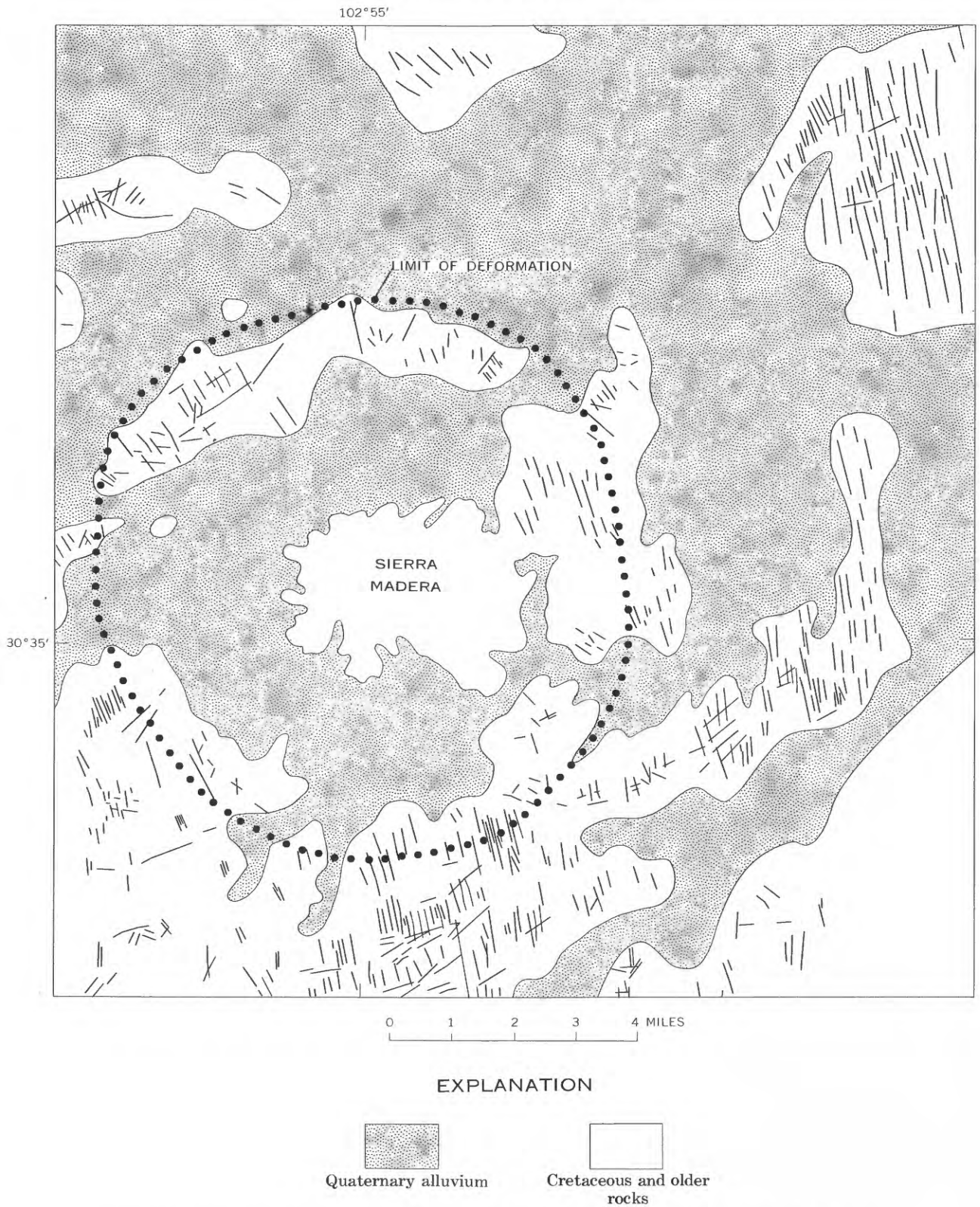

FIGURE 5.—Generalized lineaments in the vicinity of Sierra Madera. Drawn from aerial photographs.

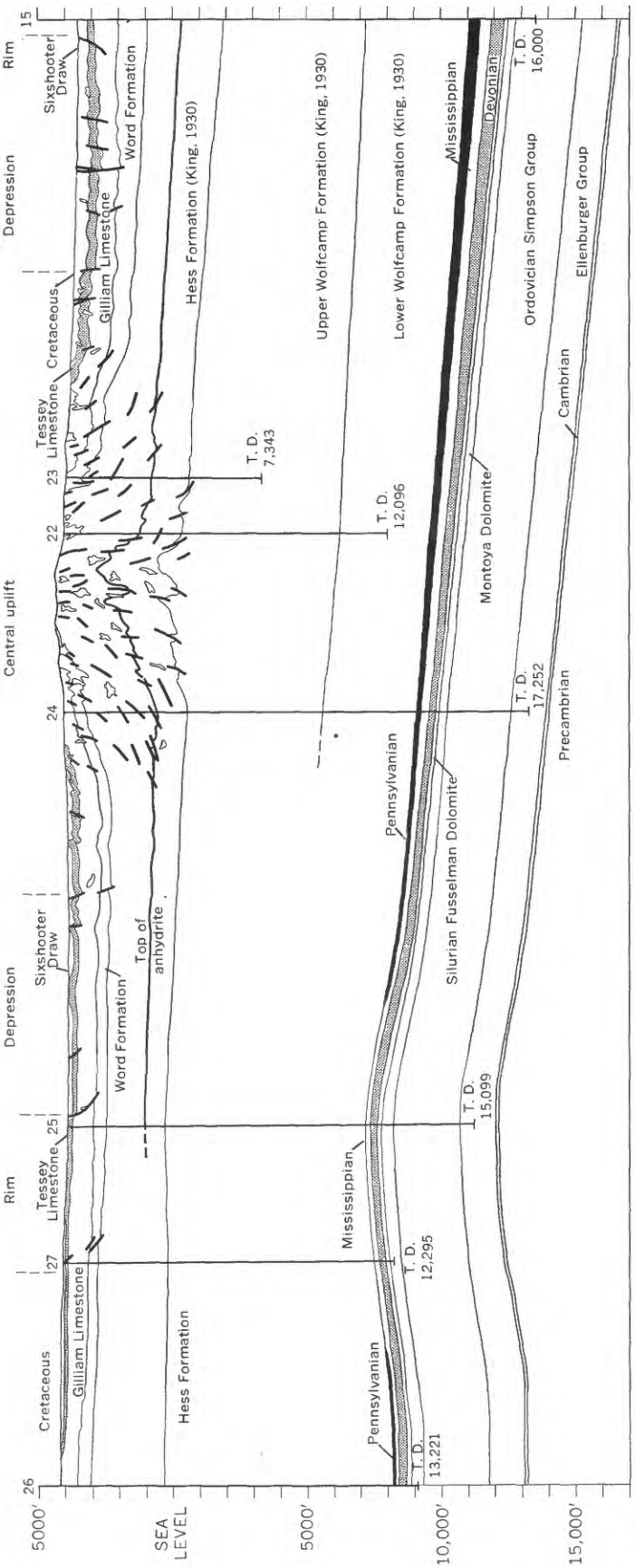

FIGURE 6.—Generalized southwest-northeast structure section across Sierra Madera. Section line connects drill holes shown on plate 2. Wells are: 15, Hunt Oil Elsinore 51; 22, Phillips Petroleum Elsinore 1; 23, Thompson (full name not known) Elsinore 1; 24, Hunt Oil Elsinore 48; 25, Hunt Oil Elsinore 52; 26, Hunt Oil, Fulk 1; and 27, Hunt Oil Elsinore 53. T.D. indicates total depth of well in feet.

of feet. Drag along faults also produced local steep dips. All the main concentric faults in the rim zone are normal faults downthrown toward the center of the structure. Displacements are generally on the order of 50 to 100 feet, but drill data (pl. 2, Hunt Elsinore 19) and exposures suggest structural relief of as much as 700 feet in some places.

The Tessey Limestone and the basal Cretaceous sandstone at their normal stratigraphic positions are exposed in the rim along its southwestern segment (pl. 2; the largest outcrop of the sandstone in the northern part of the rim may also be at its normal position), but both also form small, irregular masses along faults and other concentric fractures within Edwards Limestone. At these places blocks of Tessey dolomite (most of which contain shatter cones) and pods of overlying sandstone occur above their normal levels on both sides of the faults.

RING DEPRESSION

The ring depression separating the outer rim and central uplift is largely buried under alluvium, but drill holes (pl. 1) and exposures on the southeast side (pl. 2) show that it is floored mainly by Lower Cretaceous rocks. The largest exposures as well as the drill data reveal much disturbance, with dips up to vertical and some faulting. The depression is separated from the outer rim by concentric normal faults but is not separated from the central uplift by any significant change in style of deformation.

CENTRAL UPLIFT

STRUCTURAL FRAMEWORK

Drill-hole data and exposures indicate that strata were lifted above their normal regional levels in the central uplift across a width of 5 miles (pls. 1, 2). Inward from the ring depression the rocks are increasingly uplifted until, in the complexly folded and faulted core of the structure, the Hess Formation lies 4,000 feet above its normal level. Folds and faults are more abundant toward the center, and dips and fold plunges steepen, so that they are near vertical to overturned in a central zone about a mile wide. Despite the extreme complexity of faulting, the structure is coherent enough that the term "megabreccia" (Eggleton and Shoemaker, 1961) is inappropriate. Steeply plunging radial folds, in places broken or crushed by faults, dominate the interior. Farther out are concentric as well as radial folds; these are also broken by numerous faults.

The uplift has approximately radial symmetry. Perhaps because of the slight regional northeast dip, the Gilliam-Tessey contact outlines an oval, slightly elongate east-west, and farther in, the top of the Hess outlines an oval elongate to the northwest (pl. 3). Exposures of Hess varicolored beds in the core of the structure indicate that the greatest uplift is slightly northwest of the center of the concentric outcrop patterns. The most extreme variations in deformation around the uplift are in the complex faulting and thickening of the Gilliam on the east side (pl. 3). However, even these variations do not greatly mar the gross radial symmetry, so that the folding and faulting are classifiable into concentric zones which coincide with outcrop belts of the formations. Nevertheless, there are significant relationships between lithology and deformational style, as described below.

STYLE OF DEFORMATION

Response of the various rock units to the deformation varied according to their massiveness and competence. Massive dolomites of the Vidrio Limestone Member, Tessey Limestone, and much of the Hess Formation are slightly less convoluted than adjacent better bedded strata. The Gilliam-Tessey contact, which is fairly straight for considerable strike distances, shows only gentle undulations, and folds outlined by the Vidrio are generally larger and more open than those in the overlying Gilliam (pl. 3). Within the Tessey Limestone, structure is difficult to unravel because much of the formation is a reef breccia with high initial dips or is otherwise poorly bedded. Most observable folds in the Tessey are small and open. This is illustrated on plate 3 by the contrast of open folds in the Tessey and tight folds in the Gilliam in the same area, as at coordinates 350.2, 180.3 and 354.0, 194.2. In this report, all coordinates locating specific features refer to plate 3.

In the Gilliam, prominent bedding and numerous sandstone beds permit delineation of many small folds. Folds range from shallow basinlike synclines (348.3, 183.6; 345.5, 193.5), through somewhat rounded but chevronlike folds (349.7, 183.2), to nearly isoclinal folds (343.3, 183.5). The thickness of sandstone and dolomite beds is not changed significantly by folding, and all the mapped folds appear to have formed by flexural slip. Small-scale folds and parallel boudinage occur in dolomite in a few places. Because faults break many of the folds, one limb (346.7, 184.7; 346.1, 194.0) or the hinge itself (348.2, 196.0) may commonly be replaced. Faulting in the Gilliam is most intense on the east and west sides of the uplift.

Conglomerate of the Cathedral Mountain Formation and the sandstone member of the Word are distinctive key beds for tracing the structure around the subvertical core of the uplift. Their behavior may have been slightly more mobile than that of adjacent carbonate rocks. Both key beds are severely contorted, crushed, and faulted, as plate 3 shows, and in some places small pods occur considerably out of their normal

position, as if they had been dragged or even injected. The Cathedral Mountain conglomerate forms boudins several feet across at one place (345.8, 187.7) and locally has small-scale internal folds.

Considerable disharmony in the folding is illustrated by the anticline (fig. 7) at the top of the Vidrio Limestone Member of the Word Formation (352.3, 186.3). This anticline is box-shaped in outline and becomes faulted and broader inward at the base of the Word. Another anticline (348.1, 192.5) is rounded (where not faulted) at the level of the Word sandstone but is angular and faulted below in the Cathedral Mountain and upper Hess. Most folds are crushed (347.1, 185.9) or broken, and some are transitional to faults (346.5, 191.6; 344.8, 189.3) or to mixed breccia along a fault (345.3, 191.0). Fragmentation of the Cathedral Mountain conglomerate and Word sandstone on the west limb of a syncline (344.8, 189.3) shows that some folds were sheared apart by crushing and thinning rather than by clean faulting. Many faults in the carbonate rocks of the uplift are clean breaks with neither gouge nor breccia.

The very complicated map pattern (pl. 3) indicates that the basal Cretaceous sandstone was highly mobile

FIGURE 7.—Vertical aerial photograph (pl. 3, coordinates: 352.3, 186.3) of radially plunging anticline in the Vidrio Limestone Member of the Word Formation (Pwv) and Gilliam Formation (Pg). Traces of beds (left and top) in thin-bedded Gilliam outline other folds. Ph, Hess Formation; Pcm, Cathedral Mountain Formation; and Pwl, limestone member of Word Formation.

during the deformation. The sandstone is extensively injected (fig. 8), mainly into overlying Cretaceous limestone but also into underlying dolomite of the Tessey Limestone. It forms pods and irregular dikes from a few sand grains thick to tens of feet across, at considerable distances from its normal stratigraphic position. The sandstone map pattern, compared with those patterns of Tessey Limestone and Edwards Limestone, thus shows only the gross folds. Some injections were themselves folded and perhaps faulted after injection. Original crossbedding (fig. 9) is replaced in the intrusions by intricate flow banding (fig. 10), and isolated pods have lineated or contorted boundaries (fig. 11). Commonly the injections are tightly cemented by silica and are harder than calcite-cemented sandstone from the less-disturbed exposures. The sandstone is missing from its normal stratigraphic position in places and is several times its normal thickness in others. Its mobility suggests that it was largely unconsolidated when the Sierra Madera structure formed.

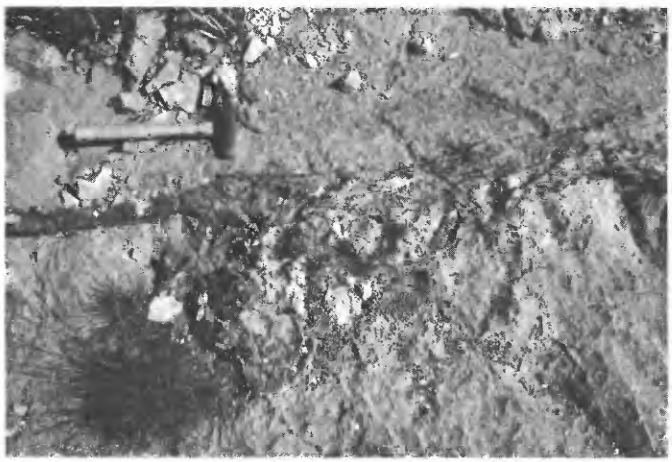

FIGURE 8.—Thin dike of basal Cretaceous sandstone (below and approximately parallel to hammer handle) injected into Edwards Limestone.

FIGURE 9.—Undisturbed crossbedding in basal Cretaceous sandstone. Such bedding was entirely reconstituted during injections of sand.

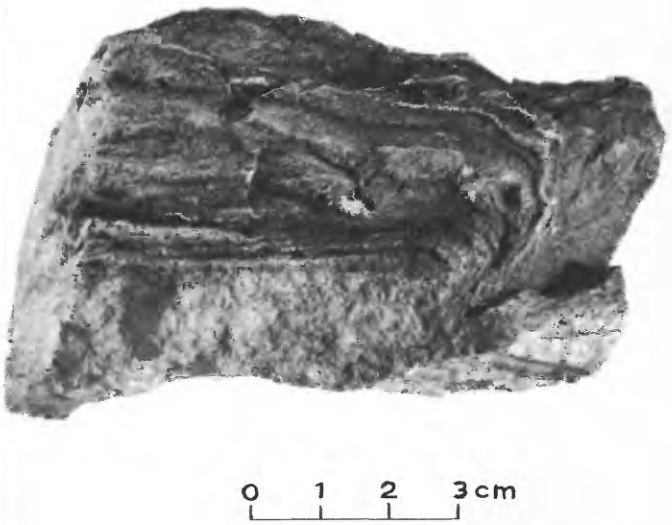

FIGURE 10.—Hand sample of basal Cretaceous sandstone from an injected mass, showing contorted flow banding.

FIGURE 11.—Irregular dike injection of basal Cretaceous sandstone showing flow foliation parallel to dike wall (top of photograph).

Where the basal Cretaceous sandstone is entirely removed from its normal stratigraphic position, typical Edwards Limestone is separated from the underlying Tessey by a few inches to several feet of sandy limestone breccia. In the limestone clasts the laminae are severely contorted (fig. 12) as though the clasts were unconsolidated when incorporated in the breccia. In such places, as well as in other structurally complex areas of Tessey Limestone, basal Cretaceous sandstone, and Edwards Limestone, limestone dikes one-fourth of an inch to 2 feet wide and over 50 feet long occur, one of

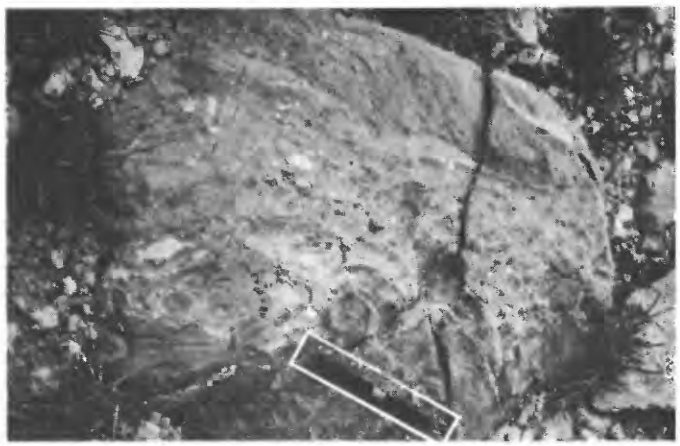

FIGURE 12.—Limestone clast in breccia separating Tessey Limestone from Edwards Limestone. Laminae internally contorted in clast.

which contains shock-deformed quartz grains. The dikes and internally contorted limestone clasts in the breccia suggest that Edwards limestones were not fully consolidated at the time of deformation. This condition, combined with the distance of Cretaceous rocks from the center of the structure, may explain the absence of shatter cones in otherwise favorable parts of the Edwards Limestone.

FOLDING

Folds in Tessey Limestone and Cretaceous rocks at the margin of the uplift are mostly a few hundred feet across. Many are quaquaversal domes and basins, so that outcrop belts form concentric patterns a few hundred feet across (pl. 3). Some of the fold plunges are gentle. Others are very steep or even inverted (339.0, 196.0; 343.8, 199.7), but even so, the structural relief is not great, as only about 600 feet of Tessey and Cretaceous strata is exposed across an outcrop width of about 4,000 feet. Circumferential folds predominate in the northeast, and radial folds, in the east and southeast. However, axial trends are not uniform, and axial surfaces are mostly curved. Some folds branch (340.5, 194.9; 342.0, 193.7). The curved axial surfaces, branching folds, and domes and basins may result from interference of radial and circumferential folding, but there is no consistent sequence. Some asymmetric and rare overturned circumferential folds in the Tessey step up toward the core of the structure.

In the Gilliam Limestone most folds are either roughly circumferential or radial to the center of the uplift. Several folds have markedly curved axial traces (353.5, 186.7; 342.3, 187.1), and in several areas folds have different axial trends (351.7, 185.0; 350.0, 183.3). Most axial surfaces dip steeply, and a few folds of circumferential trend are overturned either outward or inward. The dips of axial surfaces of some adjacent synclines and anticlines differ by 20°. If the folds formed before major tilting, their axial surfaces dipped outward. Where asymmetric, the circumferential folds in Gilliam beds step up toward the uplift, suggesting relative inward movement of upper beds over lower. Uplift and tilt were almost certainly under way when the folds were being formed, but many of the folds must have acquired their shape and symmetry at an early phase before they were much tilted.

In the Cathedral Mountain and Word Formations, most folds are radial, though there are a few tight circumferential folds (345.5, 190.8). The inward transition from mainly circumferential folds in the Gilliam to radial folds is well shown on plate 3. Radial folds in the Word Formation plunge steeply, so that the map pattern approximates the down-plunge profile. Contrary to what might be expected from the northeastward regional dip, folds on the south side of the structure generally plunge more steeply than those on the north; some plunge at angles greater than vertical (345.0, 188.2; 346.9, 191.3). Broad anticlines on the south side are separated by extremely tight, faulted synclines where Cathedral Mountain conglomerate was squeezed deep toward the center of the uplift. Such folding indicates that these strata were crowded together more than rocks farther out on the flanks. A few steeply plunging, near-circumferential folds (345.3, 191.0; 347.5, 191.7; 347.1, 185.9) may reflect such crowding of folds that were originally more radial.

Structural details within the exposed Hess Formation are poorly known because of the scarcity of marker beds and the rapid facies changes. Bedding attitudes and form lines indicate considerable disharmony and complexity. Intricate repetition is such that steeply dipping beds representing only 1,200 feet of the Hess Formation fill an area at least a mile wide. Varicolored beds near the base of the exposed sequence form convolute outcrops or discontinuous fault slivers in which the direction that the beds face is mostly uncertain. The concentric outcrop patterns apparently express steep, faulted, spinelike basins and domes (as at 349.0, 187.8; 349.6, 187.8). A complexly faulted and brecciated exposure of Cathedral Mountain surrounded with steep contacts by the Hess Formation may represent one such basin, west of the center of the structure (349.5, 186.5). The spinelike folds in the core of the central uplift are perhaps analogous to those in the core of the Grand Saline salt dome that were described by Muehlberger (1959).

FAULTING

In upper Permian and Cretaceous rocks on the outer flank of the uplift faults are few in number and generally

of small displacement. The intensity of faulting increases inward dramatically. It is complex in the Gilliam Limestone (pl. 3). In the core of the uplift the discontinuity of varicolored beds of the Hess Formation demonstrates relatively great displacements along steep faults, but nowhere great enough to expose the anhydrite beds that occur a few hundred feet below the varicolored beds in the undisturbed stratigraphic section. Throughout the structure many of the faults have no systematic pattern but appear to have formed irregularly as late adjustments to folding.

Most faults dip steeply. Curved fault traces in Word and older rocks mostly indicate not topography but curvature which was either original or caused by later folding. Low-angle faults occur in only a few places.

Along subradial faults, true directions of slip are generally unknown, but the displacement would be least if the slip were mainly perpendicular to bedding. Thus, strike slip is thought to characterize most of the subradial faults that cut steep beds in the uplift (with some exceptions, at 346.3, 191.2; 344.8, 190.7). The most prominent example is a fault in the northeast that offsets the Word Formation over a thousand feet right-laterally. Imbrication of Word and Cathedral Mountain Formations across subradial faults is thus ascribed, like the steeply plunging folds, to crowding caused by centripetal inward movement. If formed before much tilting, some subradial faults may initially have had mainly dip-slip displacements, now rotated into a strike-slip geometry. Faults on the uplift flank that bound folds of Vidrio protruding into Gilliam (346.8, 194.8; 346.1, 194.0) are best explained by such dip-slip displacement.

Circumferential faults are best seen in the Gilliam outcrop belt; most have dip-slip displacement. However, one with strike-slip displacement is suspected where the axial trace of a large syncline is offset (346.7, 185.6). The circumferential faults generally dip more steeply than bedding; thus, if they have been tilted, they originally dipped outward. Along most of the circumferential faults, strata are cut out rather than duplicated, and the center of the uplift is displaced upward relative to the flanks. This relationship is opposite to the sense implied by asymmetric folds. At one locality such a fault cuts out concentric isoclinal folds (345.4, 190.8) and therefore is later. Thus, repetition by folding due to inward movement of upper beds over lower appears to have been followed by upward movement of the uplift core pulling away from the flanks by faulting.

Very few thrust faults are proved, contrary to an earlier conclusion based on mapping of a small area (Shoemaker and Eggleton, 1964). One flat-lying fault displaces the Word Formation over the Hess Formation. Other thrusts displace older rocks outward over younger ones on the north (fig. 13) and east (349.0, 196.8; 347.9, 194.2) sides of the uplift. The northern thrust (fig. 13), which displaces Vidrio on overturned Gilliam beds, is bounded on the west side by a strike-slip fault that curves around behind to become a major normal fault bounding the thrust block as if it were a large outward-directed slump. The thrusts suggest that the Vidrio rose until outward movement became easier than vertical movement. The situation may be analogous to the formation of a mushroom cap when a diapiric mass completes its penetrative rise.

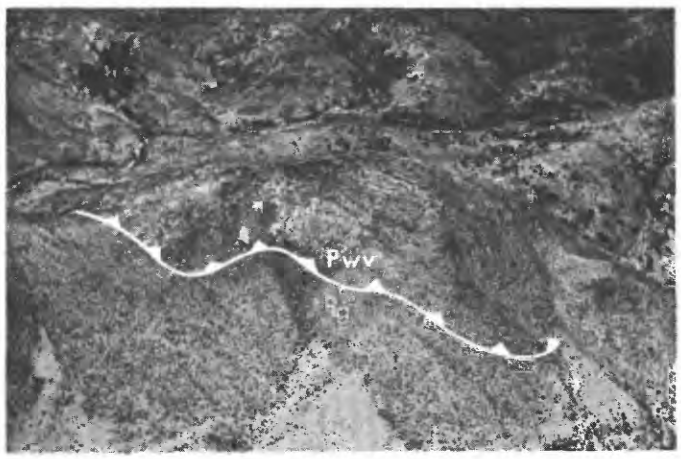

FIGURE 13.—Oblique aerial photograph showing part of low-angle thrust with the Vidrio Limestone Member of the Word Formation (Pwv) structurally overlying the Gilliam Limestone (Pg) (pl. 3, coordinates 351.4, 187.3).

SUMMARY OF CENTRAL UPLIFT

The geometry of the central uplift suggests that it formed by inward as well as upward movement of strata (Wilshire and Howard, 1968). Individual beds, exemplified by the Cathedral Mountain Formation, are duplicated by faulting and folding so that the total strike length of the beds is greater than the length of the perimeter on which they lie; the perimeter at the stratigraphic level of the Cathedral Mountain was evidently shortened about 25 percent by inward movement during doming. Moreover, the section in the center is thickened by repetition so that near-vertical beds representing only 1,200 feet of Hess strata fill an area with a minimum width of a mile, and the Phillips drill hole near the center of the structure (pl. 2) shows that the thickening persists below the surface and is thus more than superficial. The rocks are not sufficiently bulked by brecciation to otherwise account for the volume of uplifted rocks, so the fact that the structure narrows and dies out at depth requires that the uplift volume be accounted for by inward movement of the strata involved.

Faulting and radial folding are believed to be a consequence of this inward and upward motion. Just

as with a napkin being pulled up through a ring or with salt flowing into a diapir (Balk, 1949), crowding together of strata by this centripetal movement produces radial folds that plunge down the flanks (fig. 14), and produces subradial faults. The intense faulting, as compared with internal structures of salt domes (Balk, 1949), surely results in part from the greater rigidity of the rocks at Sierra Madera but also suggests that deformation was rapid.

The circumferential folds and complex branching, crossing, and domical folds that dominate the flanks of the uplift suggest irregular adjustments to compression and inward movement of upper beds over lower, as if centripetal motion of the uppermost beds had dragged lower strata inward and upward. Circumferential faults then formed that have an opposite sense of movement, indicating that the center of the uplift was pulling upward away from the flanks. Spinelike faulted folds may have formed in the uplift core at this stage. The few outward-directed thrusts may have formed late in the sequence by gravitational spreading of the rising dome.

The ring depression formed in response to tectonic thinning accompanying the inward movement of rocks to form the central uplift. This feature resembles the rim synclines which surround many salt domes (Nettleton, 1955; Parker and McDowell, 1955). Thus, in several respects, Sierra Madera resembles diapiric structures, but, for reasons discussed later, diapirism is not a tenable explanation for the structure. The inward motion that formed the uplift is also recorded by the normal faults that drop rocks down from the rim into the ring depression. It is unknown, however, whether downdropping along these faults caused the inward motion and the uplift or whether the uplift caused the rim faults by withdrawal of material from the ring depression.

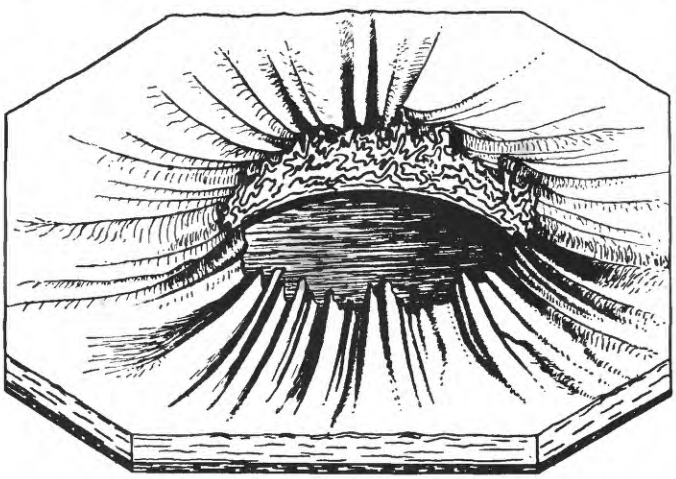

FIGURE 14.—Diagram (from Balk, 1949) illustrating radial folds on top of a salt bed formed by centripetal inward movement into a salt dome; pattern is comparable to folding in the central uplift of Sierra Madera. The cut along the hypothetical vertical cylinder shows inferred internal structure of the salt.

SHOCK DEFORMATION

Brecciation, shatter cones, and certain types of internal structures of minerals at Sierra Madera are ascribed to shock deformation. There are two types of deformational breccia: one composed of fragments of only one lithology, the other of fragments of several lithologies. Shatter cones, a very common mode of rock failure in cryptoexplosion structures, are well developed in Permian rocks at Sierra Madera. Within the area in which breccias and shatter cones occur, quartz grains commonly have cleavages and other planar elements characteristically formed by shock. Calcite and dolomite are also deformed but were not examined closely.

MONOLITHOLOGIC BRECCIAS

The more common of the two types of deformational breccia is composed of only a single lithology. The distribution of well-developed monolithologic breccias is shown in figure 20, but less obviously brecciated rock is considerably more widespread on the central uplift than illustrated. Lower Cretaceous rocks are only rarely brecciated (fig. 15), consistent with the suggestion made before that they were not fully consolidated at the time of deformation.

Except for original sedimentary breccia in the Tessey Limestone (well displayed in the Glass Mountains), brecciation at Sierra Madera suggests intense shattering and is unique to the region. In places, the deformational brecciation is clearly superposed on Tessey sedimentary brecciation.

Incipient brecciation in Permian rocks at Sierra Madera is marked by widely spaced, thin (generally

FIGURE 15.—Monolithologic breccia of basal Cretaceous sandstone.

less than 0.5 millimeter), irregular veinlets of mylonite. An electron micrograph indicates that the mylonite is composed of very tightly packed, angular grains of carbonate a few microns long. In a more advanced stage of brecciation, mylonite veinlets, less than 0.5 mm thick, form an intricate intersecting network that separates unrotated clasts as much as 2.5 cm long (fig. 16). Clasts more than a few millimeters long are internally shattered, and the cracks filled with mylonite. The mylonite in such breccias does not weather out differentially from the clasts, and the rocks generally are not recognizable as breccias in the field. The most advanced stage of brecciation is represented by rocks in which the mylonite weathers out differentially, so that the clasts are conspicuous in outcrop (fig. 17).

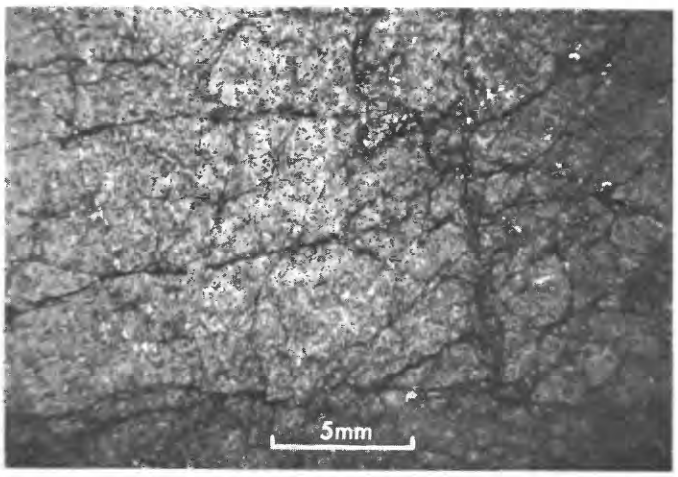

FIGURE 16.—Photomicrograph of intermediate stage of monolithologic brecciation showing unrotated clasts in network of mylonite veinlets.

FIGURE 17.—Monolithologic breccia of dolomite from the Gilliam Limestone. These thoroughly shattered beds grade laterally (outside the photograph) to unbrecciated dolomite with no change in form and smoothness of bedding-plane partings.

TABLE 3.—*Partial chemical analyses of clasts and matrices of monolithologic breccias*

[Analyst: J. A. Thomas. Ca and Mg by colorimetric titration, Fe by atomic absorption. Results in percent except for molal ratio]

Formation or Member	Ca	Mg	Molal ratio	Total carbonate	Fe_2O_3
Tessey:					
Clast	21.7	12.7	1.04	98.4	0.195
	22.5	12.4	1.10	99.3	.330
Matrix	21.6	12.2	1.07	96.3	.197
	22.7	11.8	1.17	97.7	.445
Gilliam:					
Clast	21.6	12.9	1.02	98.8	.130
	20.7	12.3	1.02	94.5	.175
	22.4	12.2	1.11	98.3	.225
Matrix	22.1	12.8	1.05	99.7	.182
	21.8	12.7	1.04	98.6	.210
	21.8	11.8	1.12	95.4	.225
Vidrio:					
Clast	21.8	12.2	1.08	96.8	.100
Matrix	22.7	12.2	1.13	99.1	.100

Staining of cut slabs and partial chemical analyses (table 3) of mylonite and clasts indicate very small compositional differences. In well-bedded rocks such as the dolomites in the Gilliam Limestone, pervasive brecciation had no effect on the spacing and smoothness of bedding-plane partings (fig. 17). Clast sizes range from a few centimeters down to grain size of the original rock (fig. 18), and the size distribution appears to vary randomly, both vertically and horizontally in individual beds. As in the intermediate stage of brecciation, clasts larger than a few millimeters are typically shattered (fig. 20) and the cracks are filled with mylonite. Mylonite between clasts makes up as much as 30 to 40 percent of such breccias and is commonly laminated

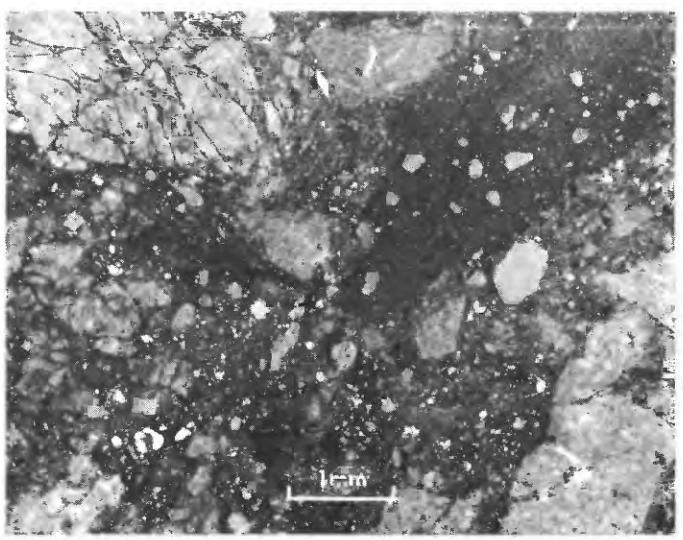

FIGURE 18.—Photomicrograph of monolithologic breccia of dolomite from the Tessey Limestone showing extreme clast-size variation, extensive internal shattering of clast (top left), and thin finger (diagonal from top right) of darker, finer grained mylonite with internal flow foliation.

parallel or subparallel to clast boundaries; small elongate rock fragments are also oriented parallel to larger clast boundaries (figs. 18, 19). Since the mylonite veins and clasts are variously oriented in a particular rock, such laminations (caused by grain-size variations) and fragment orientations must have been produced by flow of the mylonite. Preservation of original bedding-plane partings, however, indicates that only small movements are required for the size sorting and grain orientation.

Tessey sedimentary breccias are characterized by a homogeneous matrix in which detrital quartz is concentrated and by little change in grain size between clasts and matrix, so that clast boundaries are vague. The matrix generally has a moderate proportion of exceedingly fine-grained carbonate(?) along with more abundant carbonate of nearly the same grain size as in the clasts. In contrast, the deformational breccias are characteristically flow-banded and vary greatly in grain size; clasts are sharply bounded and internally shattered, and detrital quartz is uniformly distributed in clasts and matrix. These features suggest that the deformational breccias formed by shattering and cataclastic flow. Of the several types of breccias in carbonate rocks described by Blount and Moore (1969), only the fault breccias bear much resemblance to those at Sierra Madera. Most monolithologic breccias at Sierra Madera, however, are clearly unrelated to faults (fig. 20).

Monolithologic breccias (fig. 20) occur generally within the zone of shatter cones. (See fig. 30.) Generally these breccias contain only trace amounts of quartz, which is undeformed; carbonate minerals are deformed in some monolithologic breccias but not in others. The physical characteristics of the monolithologic breccias suggest tensile shattering, perhaps caused by the rarefaction phase of a shock wave.

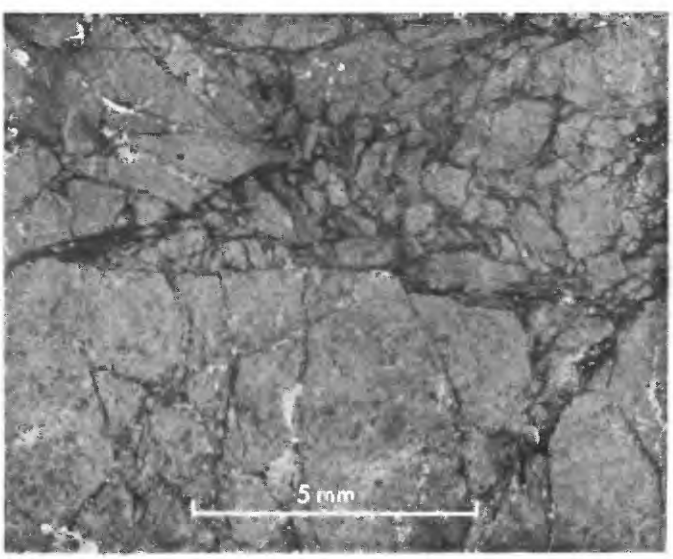

FIGURE 19.—Photomicrograph of Vidrio monolithologic breccia showing internal shattering of clasts.

MIXED BRECCIAS

The second type of deformational breccia at Sierra Madera is composed of clasts of two or more lithologies, either from the same or different formations. Clasts of monolithologic breccias also are present. Mixed breccias occur in all formations on the central uplift, but they form considerably larger masses and are more abundant in the older rocks (fig. 20). These breccias form steeply dipping tabular sheets, 1 to 150 feet thick and 100 to 1,700 feet long, and irregular masses as large as 1,100 feet across. Most of the mixed breccias appear to crosscut the country rock at steep angles, but gradations to monolithologic breccia are locally present. Some tabular sheets of breccia were clearly emplaced along faults, whereas others were emplaced along bedding planes that now dip steeply. In one place (353.1, 189.5), the top of a thin steeply dipping sheet of breccia connects with a large irregular breccia mass; the latter appears to be approximately concordant with local bedding in the Gilliam, as though it were a sill with a dike feeder. Other irregular breccia masses, however, clearly crosscut the country rock and show small-scale intrusive relations to it (fig. 21). At one locality the country rock at its contact with mixed breccia is slickensided, and striae plunge nearly down the 75° dip of the contact.

Steeply dipping flow foliation is locally conspicuous, especially in tabular sheets of breccia but also in some irregular masses. The flow foliation is expressed by orientation of elongate and slabby rock fragments and by size sorting of clasts to produce a repetitive layering parallel to the walls of the breccia masses. Locally, there is a crude size sorting of clasts, such that generally smaller ones are concentrated near the breccia margins, and one thin breccia sheet has a prominent central concentration of large clasts (fig. 22). These relationships indicate emplacement of the breccia masses as dense suspensions of clasts and finely comminuted rock debris, probably in CO_2-rich water or water vapor. The tendency for axial migration of solid particles under possibly comparable conditions of flow is well known (Simkin, 1967), and Wilshire (1961, 1969) has suggested that repetitive size-sorted layers may form by shear flow in dense suspensions of particles in fluid. In one place, very fine-grained sandstone veinlets crosscut marginally flow-foliated breccia. The veinlets may represent late injection of softened and disaggregated inclusions into fractures in the breccia. (Similar phenomena in diatremes were described by Wilshire, 1961.)

The mixed breccia is hard, dense rock, difficult to break with a hammer. The cement of the clasts is

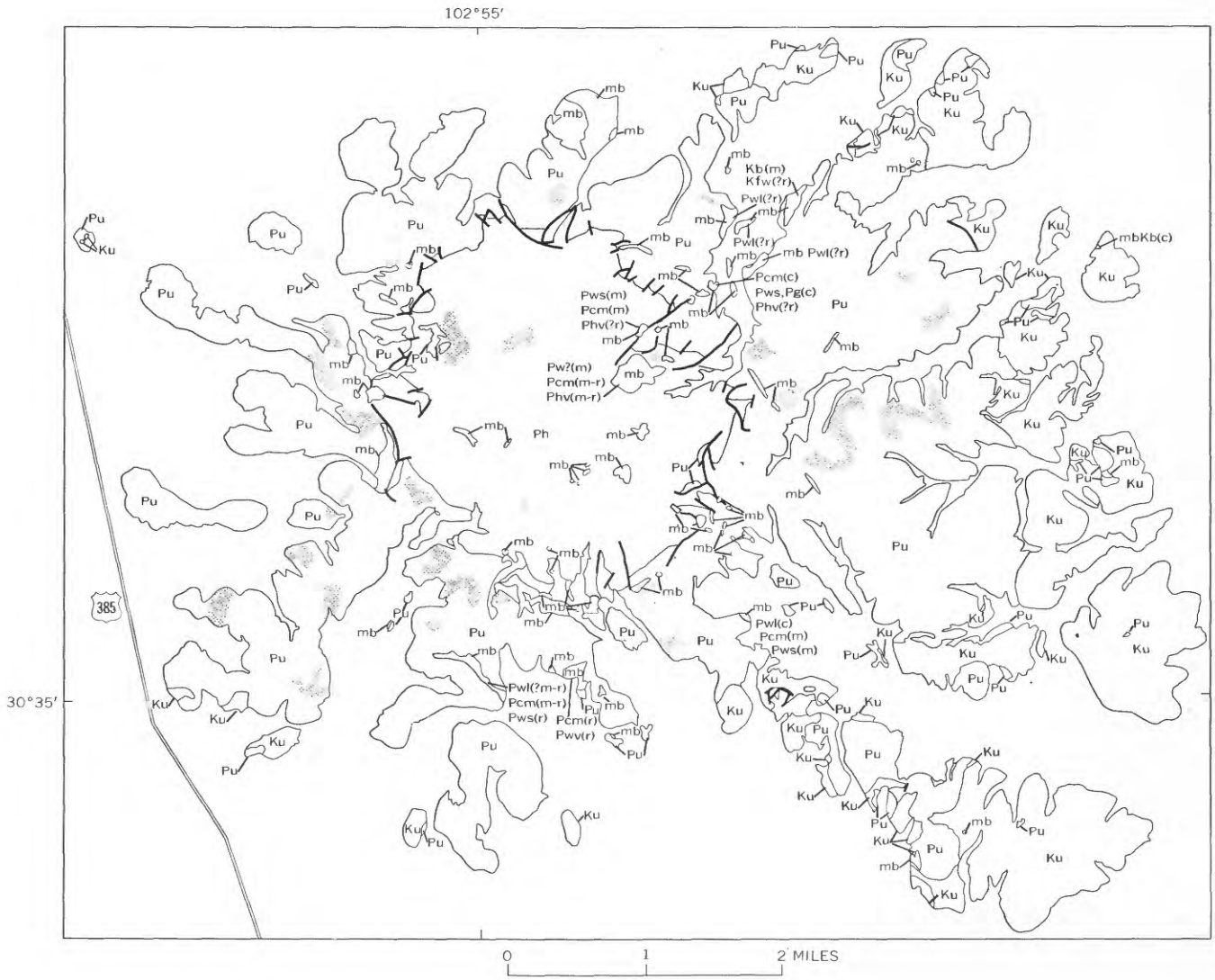

EXPLANATION

mb — Mixed breccia

Abundance of fragments is shown in parenthesis by c, *common;* m, *moderately abundant; and* r, *rare. Source of fragments, other than from adjacent formations, is shown by the following symbols:* Ke, *Edwards Limestone;* Kb, *basal Cretaceous sandstone;* Pt, *Tessey Limestone;* Pg, *Gillian Limestone;* Pwv, *Vidrio Member, Word Formation;* Pws, *sandstone member, Word Formation;* Pwl, *limestone member, Word Formation;* Pcm, *Cathedral Mountain Formation;* Ph, *Hess Formation;* Phv, *Varicolored beds, Hess Formation*

Monolithologic breccia

Ku — Cretaceous rocks undivided

Pu — Permian rocks undivided, exclusive of Hess Formation

Ph — Hess Formation as used by King (1930)

FIGURE 20.—Simplified map of central uplift showing distribution of mixed breccias and of clasts derived from formations other than that formation in which the mixed breccia is located. Stipples show areas of well-developed monolithologic breccias.

FIGURE 21.—Small intrusion of mixed breccia (light, bottom of photograph) into steeply dipping sandstone unit of Gilliam Limestone. Two thin dark bands in sandstone are truncated by apophysis of mixed breccia. Dolomite in the Gilliam at and above hammerhead.

FIGURE 22.—Sample from thin dike of mixed breccia showing central concentration of large clasts.

typically a rust-colored, exceedingly fine-grained carbonate in which individual grains cannot be clearly resolved with the microscope. The cement may represent slightly recrystallized rock powder rather than a later chemical deposit.

Wherever mixed breccias occur, the dominant clasts were derived from the immediately adjacent formation. Many of them, however, also contain clasts derived from other formations (fig. 20). Because of the general similarity of lithologies, only fragments of such formations as the Cathedral Mountain, the sandstone member of the Word, and the Cretaceous basal sandstone could be consistently identified as foreign. Foreign fragments range from common to rare; in one example, the breccia consists almost entirely of broken red dolomite from the Gilliam derived from immediately adjacent beds with a few scattered quartz and chert pebbles from the Cathedral Mountain Formation, separated about 1,000 feet stratigraphically from this part of the Gilliam. Figure 20 shows that fragments derived from formations other than the one in which the breccia occurs have moved both upward and downward stratigraphically for stratigraphic distances of as much as 1,700 feet. The direction and true distance of movement of such fragments, however, are not known.

A common clast in mixed breccias in the Gilliam and older rocks is white silty claystone. The clay, which is optically nearly isotropic, was identified as kaolinite by X-ray. Some such clasts are deformed (fig. 23). No rocks of this lithology are exposed at Sierra Madera, and their source is unknown.

Another common constituent of mixed breccias is unbroken, commonly fossiliferous, chert nodules. That these are products of replacement of limestone clasts after brecciation is clear from the gradation between chert with small, irregular limestone cores to very thin chert rinds on limestone clasts. Associated with these chert nodules in a few mixed breccias are octahedral crystals as much as 1½ inches across, some of which show penetration twins. These crystals were probably originally fluorite but are now entirely replaced by very fine grained quartz and carbonate. Silification of limestone clasts and fluorite as well as cementation of the breccias by fine-grained carbonate indicates that the mixed breccias were considerably modified after they were emplaced. Alteration was probably accomplished by ground water or by fluids in which the comminuted rock was carried.

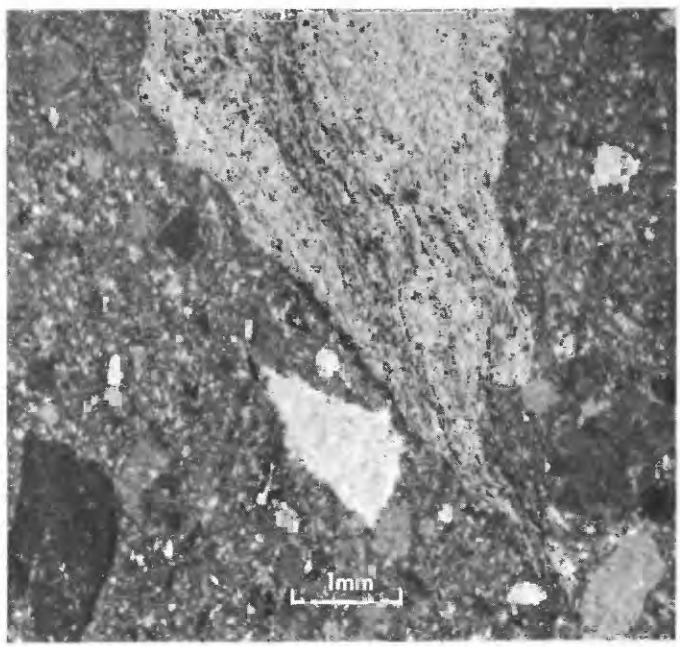

FIGURE 23.—Photomicrograph of deformed foliated claystone clast in mixed breccia.

Another type of chert clast, found only in the mixed breccia near the center of the structure at the Phillips well site (pls. 2, 3), is of special interest because of its well developed flow structure (fig. 24). Seventeen such specimens were collected from the breccia, some of which have poorly preserved fusulinids that may have been derived from the Word Formation (R. C. Douglass, written commun., 1969). If derived from the Word, such fragments are below their normal position in breccia composed mainly of the adjacent Hess strata. The clasts are composed almost entirely of fine-grained quartz, but voids conspicuous in some specimens are locally filled with calcite and rare fluorite. In hand specimen, the fusulinids (up to 1 inch long) range from undeformed to almost unrecognizable forms smeared out in a foliation; probably at least part of the foliation is a result of thoroughly smeared fusulinids. The foliation is generally curved, and linear streaking is also conspicuous, so that specimens resemble stretched taffy or volcanic bombs. Thin sections (fig. 25) show clearcut evidence of fluidal flow, despite complete recrystallization to fine-grained quartz mosaics. The larger quartz grains typically have a pronounced zoned or radial extinction that suggests recrystallization of spherulites. In contrast to other quartzose clasts in the mixed breccia, the quartz and calcite of these flow-foliated clasts contain no shock-formed planar elements. Taken together, these features suggest that such clasts may have been melted and subsequently recrystallized. However, these characteristics could also result from silicification or recrystallization of an unmelted mylonite, and somewhat similar textures were produced experimentally without melting (Carter and others, 1964).

Mixed breccias occur in all formations on the central uplift (fig. 20); thus their distribution roughly coincides with that of monolithologic breccias and shock-

FIGURE 24.—Strongly foliated, melted(?), and recrystallized chert clast from mixed breccia.

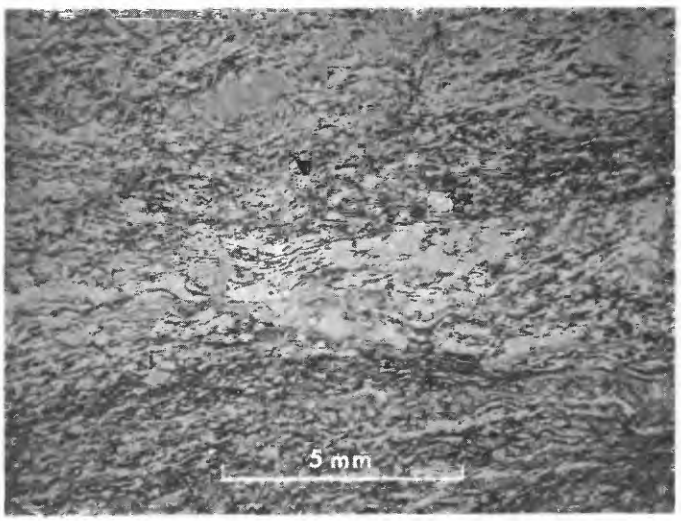

FIGURE 25.—Photomicrograph of foliated chert clast showing fluidal flow features. Light areas are more coarsely recrystallized quartz.

deformed quartz. (See fig. 31.) Unlike the monolithologic breccias, the mixed breccias contain quartz that has been subjected to intense shock deformation. The occurrence of some mixed breccia bodies along faults and the common occurrence of clasts of monolithologic breccia and broken shatter cones in these breccias suggest that much of the mixed breccia was emplaced during folding and uplift. Because of folding and faulting, foreign fragments in mixed breccias may have moved obliquely for shorter distances than the stratigraphic separation of the source bed of a foreign fragment and the formation in which the host breccia is now found. The occurrence together of foreign fragments derived from stratigraphically both above and below the formation in which the breccia is found suggests that probably very transient dilational or shear fractures were propagated over stratigraphic distances of as much as 1,700 feet. Fragments injected or spalled into such fractures may have been mixed by compressive pump action of the fracture walls if the radial inflow of material forming the central uplift were nonuniform.

SHATTER CONES

Shatter cones at Sierra Madera, as elsewhere, are conical fracture surfaces with characteristic striae that fan outward from the apex in "horsetail" fashion (fig. 26; Howard and Offield, 1968). The striae are sharp grooves between intervening rounded and broader ridges; they are straightest, most regular, and best developed in fine-grained rocks; in coarser rocks they are coarser and less detailed. Away from the apex, the surface of a cone is built up by parasitic cone segments successively overlapping like shingles. Whole cones and clusters of whole cones having a common axial orientation are found in places (fig. 26*A*), but segments or

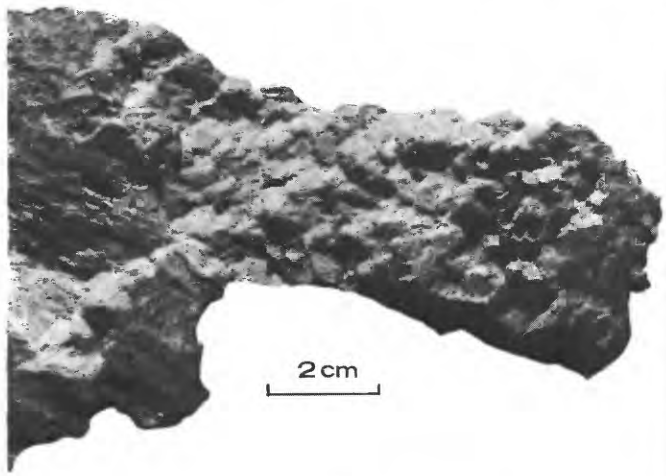

A

B

FIGURE 26.—*A*, Whole shatter cones, 2 to 10 millimeters high, in marly dolomite of Gilliam Limestone; length of specimen 11 centimeters. *B*, Variously oriented shatter-cone segments in marly dolomite of Gilliam Limestone. Surfaces in foreground and background are parallel and have similarly oriented cone segments. Note shinglelike overlap of parasitic cone segments. Specimen 6.5 by 5.5 cm.

partial cones (fig. 26*B*), which may intersect at high angles, are more common. Cone segments may have any orientation relative to bedding; in several places, particularly in aphanitic dolomite, they are preferentially developed on joint and bedding surfaces, so that in outcrop they may be developed almost exclusively on two or three sets of such subplanar surfaces. Some whole cones are asymmetric, having one side longer than the other.

Shatter cones are found in all the exposed Permian formations. Figure 27 shows their outer limit of abundance on the central uplift. The distribution of cones is very irregular, partly because lithology is an important factor in their formation; fine-grained and brittle rocks appear to have been most favorable. Thus cones are most common in aphanitic and dense marly dolomite; are present in crystalline dolomite, siltstone, fine-grained sandstone, and calcareous chert; are least common in limestone; and do not occur in coarse-grained sandstone. They may, however, be abundant in a particular rock type at one place and not be developed at all in virtually the same lithology at another place.

Whole cones range in height from less than 2 mm to 12 cm and the sides are 2 mm to 17 cm long, but incomplete cone segments are typically larger, as much as 45 cm long. Even in a single bed with 3-cm whole cones, cone segments reach 10 cm in length. For any given rock type, cones are more abundant toward the center of the structure but show no change in range of size. Along the outer limit of abundant shatter cones (fig. 27), the cone segments typically are 5 cm long in aphanitic dolomite, up to 12 cm long in marly dolomite, and up to 20 cm long in sandy siltstone; in like rocks near the center they are comparable in size.

The rocks in which shatter cones are most abundant also have generally the smallest cones. This lithologic control of size of shatter cones is illustrated in the Gilliam Limestone where sandy layers with 20-cm cone segments and finely crystalline dolomite beds with 5-cm cone segments are in direct contact. Another example is an outcrop of Word Formation, a few meters across, where finely crystalline dolomite contains a few cone segments 9 cm long, marly dolomite layers contain abundant well-developed cone segments 5 cm long, but crystalline dolomite, limestone, and medium-grained sandstone contain no cones. Aphanitic marly dolomite of the Gilliam contains cones as small as 2 mm; the longest cone segments are in sandy dolomite of the Word Formation (up to 35 cm) and limestone of the Hess Formation (up to 45 cm).

Shatter cones are not present in Cretaceous rocks at Sierra Madera, even where these rocks are in contact with marly dolomite of Tessey Limestone containing abundant cones. The absence of cones in aphanitic to medium-grained Cretaceous limestone may be due to lack of consolidation, combined with distance from the center of the structure.

Most shatter cones are within 1 to 2 miles of the center of the structure, as figure 30 shows. However, cones also occur in the uppermost dolomite of the Tessey near the east and south margins of the map (pl. 2). At the most distal locality, the rock was driven upward as a small slice into Cretaceous strata along a fault on

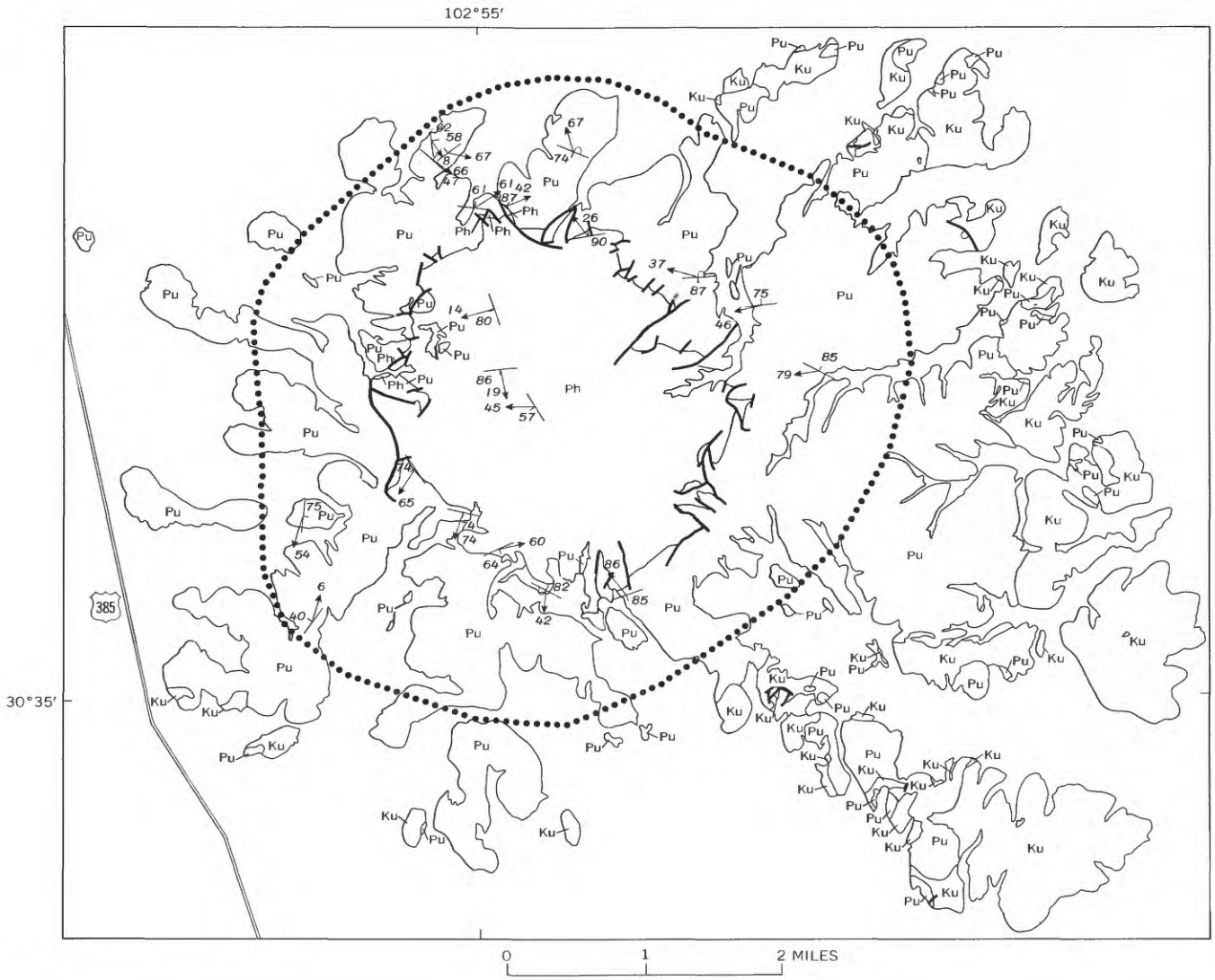

EXPLANATION

Ku — Cretaceous rocks undivided

Pu — Permian rocks undivided, exclusive of Hess Formation

Ph — Hess Formation as used by King (1930)

Outer limit of abundant shatter cones

75/34 — Strike and dip of beds containing shatter cones

Arrow shows direction of point of cones, number shows angle of cone axis measured up from horizontal

FIGURE 27.—Distribution of abundant shatter cones and orientation of shatter cones in place. Strike and dip of bedding shown by standard symbols. Direction of point of cones shown by arrows, with angle measured up from horizontal in degrees.

the outer perimeter of the structure, about 4 miles southeast of its center.

Cones also occur at depth. Cuttings from a well drilled within about 0.3 miles of the center of the structure reveal probable cone segments to a depth of 1 mile—4,000 feet stratigraphically below the top of the Permian. Possible cone segments are found from lower cuttings throughout the rest of the hole to a depth of 12,000 feet.

Axes of whole cones in clusters have a nearly common orientation in any outcrop (fig. 26). In exposures showing only segments of cones (fig. 26*B*), measurement of many striae shows that the segments are incomplete parts of cones having a common orientation and that they define a common cone axis, even though the segments themselves are at large angles to one another.

Each striation measured at an outcrop was plotted on a lower hemisphere stereographic projection with the direction of point indicated. Most plots resulted in a circular pattern corresponding to a conical arrangement of striae. Orientations and apical angles of the cones were determined by fitting small circles to these circular patterns. Figure 28*A* shows a typical plot of striae from cone segments; for comparison, figure 28*B* shows striae measured on a single whole cone from a different locality.

On average, 26 striae per locality were measured except for three localities in which whole cones were measured directly; it was found that cone geometry could be reasonably estimated from as few as eight striae.

Cone segments in a single structural block define an average cone orientation and an apical angle at most places at Sierra Madera. However, a few measured striae in one locality fall far off the circular plot, and data from three localities were discarded altogether, because striae orientations were scattered and no unidirectional cone axis was obvious. The discrepant orientations of cone segments may be attributable to effects of inhomogeneities in the rock.

Cones in a single structural block generally point in the same direction, as well as having the same axial orientation. In a few localities, however, some segments (as many as 31 percent) point in a direction opposite to the dominant direction of the cluster.

Apical angles range from 75° to 108° and average 88.5°; thus they are significantly smaller than those reported from the Vredefort ring of South Africa, where angles range from 90° to 122° (Manton, 1965). Figure 29 suggests that, as at Vredefort, each stratigraphic unit has a characteristic range of apical angles and that apical angles may be influenced by rock type.

Rocks containing shatter cones have been faulted and folded, and no pattern is obvious when the average

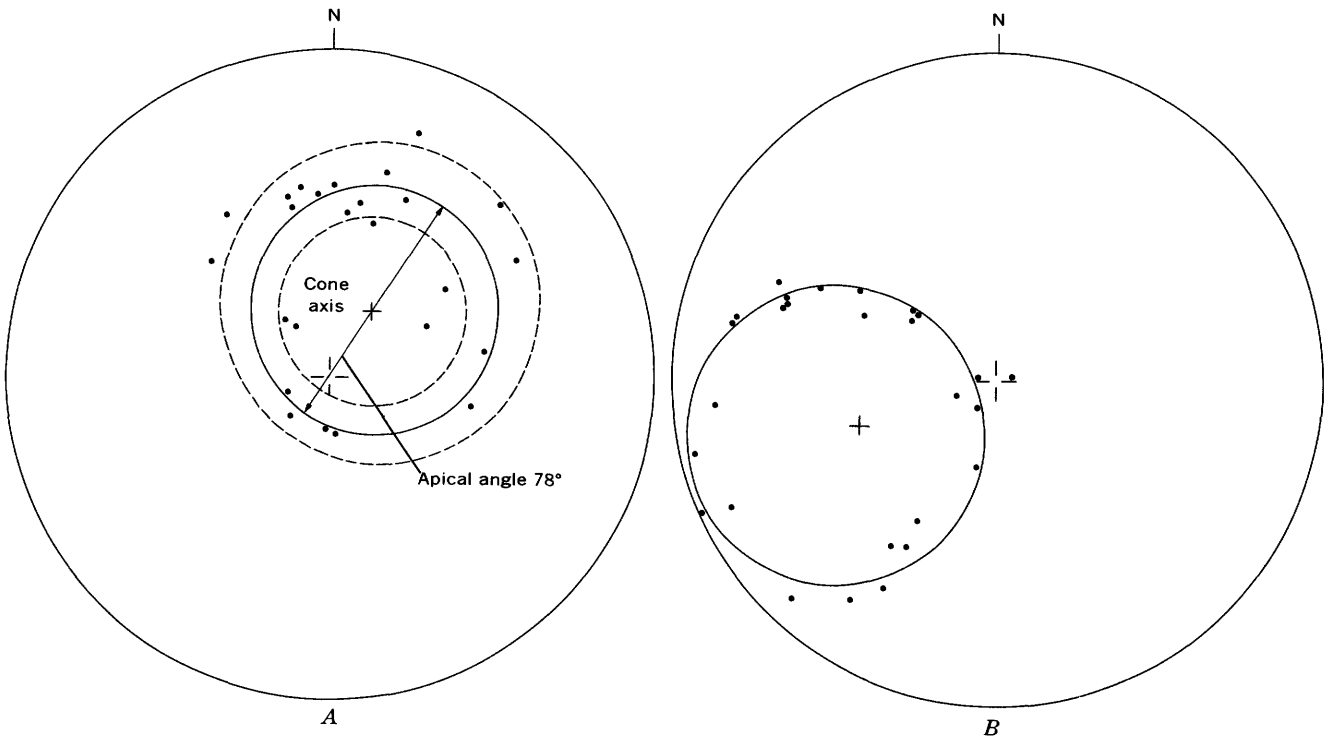

FIGURE 28.—*A*, Striae from shatter-cone segments from one locality, plotted on lower hemisphere stereographic projection (all indicate upward-pointing cones); dashed circles are drawn 10° from small solid circle selected to represent cone. *B*, Striae measured on a single upward-pointing whole cone.

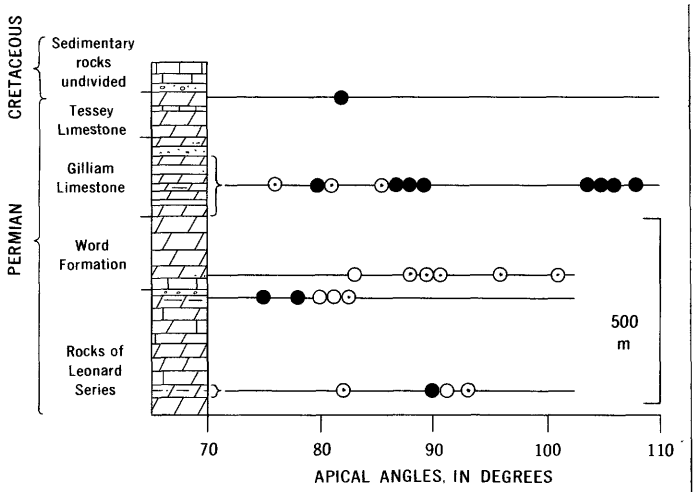

FIGURE 29.—Apical angles of shatter cones measured at various stratigraphic levels. Each measured apical angle is represented by a symbol showing rock type: dotted circles, siltstone or sandstone; solid circles, aphanitic or marly dolomite; open circles, crystalline dolomite. Rock-column symbols: rectangular brick, limestone; slanted brick, dolomite; circles, conglomerate; dots, sandy or sandstone: dashes, shaly or marly.

orientation of cones from each measured locality is plotted on a map (fig. 27). Evidence from the three northwesternmost localities, where shatter-cone orientations were measured on both limbs and the trough of a syncline, indicates that the cones formed before folding: although oriented differently at all three places, if the syncline is unrolled, the cones approach a common orientation. Likewise, some broken cones found in fault breccia show that the cones predate faulting.

The original cone orientations can be estimated but cannot be determined exactly. The paths through which they were deformed were undoubtedly complex; the initial attitudes of bedding also are unknown. Before the cryptoexplosion structure formed, Cretaceous strata lay nearly flat, but the underlying Permian rocks of the area had a small northward regional dip and gentle undulations, with dips locally as high as 20°.

Nevertheless, if the cones formed before the central uplift, their initial orientations can be approximated by assuming that the Permian beds were horizontal and that there were simple rotations. The facing direction of beds is known certainly for all but the three most central localities. Bedding orientations were rotated to horizontal about their strike lines by computer.

The resultant pattern (fig. 30) clearly shows cones pointing inward and upward, as at other cryptoexplosion structures where shatter-cone orientations have been well studied. Considering the simplifying assumptions used in restoring the beds to their initial positions, the in-and-up pattern is surprisingly good. One exception, the easternmost locality, lies in a chaotic sedimentary reef breccia where initial dips were so high that the rotation assumption is not valid. A single location of outward point, in the southwest, is representative of the minority of cones that developed along the same axes but with points opposite those of the prevailing pattern. Apart from the easternmost locality, 13 percent of all striae measured indicate cones pointing away from the center; 87 percent indicate cones pointing toward the center.

Cone-axis plunges are steepest in the center and decrease outward. A crude central focus of intersecting cone axes was found by computer after restoring the strata to a horizontal position. This approximate focus (standard deviation of 2,000 feet) occurs at the top of the Permian section directly over the center of the uplift (fig. 30).

These results generally confirm those of Manton (1965), Bray and others (1966), Stearns, Wilson, Tiedmann, Wilcox, and Marsh (1968), and Milton (1969), all of whom have shown that shatter cones in other structures point inward and upward if the beds containing the cones are restored to the attitudes they had before the structures formed.

The formation of shatter cones by shock has been demonstrated by hypervelocity impact experiments (Shoemaker and others, 1963) and at craters formed by nuclear and chemical explosions (Bunch and Quaide, 1968; Roddy, 1969a). Roddy studied craters formed by explosion of TNT spheres near ground surface. The apices of shatter cones at these craters point toward the energy source, as do those formed by the aforementioned impact experiments. The symmetry of restored shatter-cone orientations at Sierra Madera suggests that the cones were formed by a shock wave of generally hemispherical form that originated above the present ground surface and at the center of the structure.

SHOCK-DEFORMED QUARTZ

Quartz grains in many deformed rocks from Sierra Madera display multiple sets of planar structures characteristic of naturally and artificially shocked quartz (fig. 31). Carter (1968) distinguished four types of planar structures in quartz—cleavage, faults, planar features (a group of structures as yet poorly understood), and deformation lamellae. Of these, we distinguished with certainty only cleavage (fig. 32). The remaining planar structures (fig. 33) in quartz from Sierra Madera are hereafter referred to collectively as "planar elements."

Multiple sets of planar elements in individual grains of quartz were first discovered at Sierra Madera by N. M. Short (written commun., 1966). We have exam-

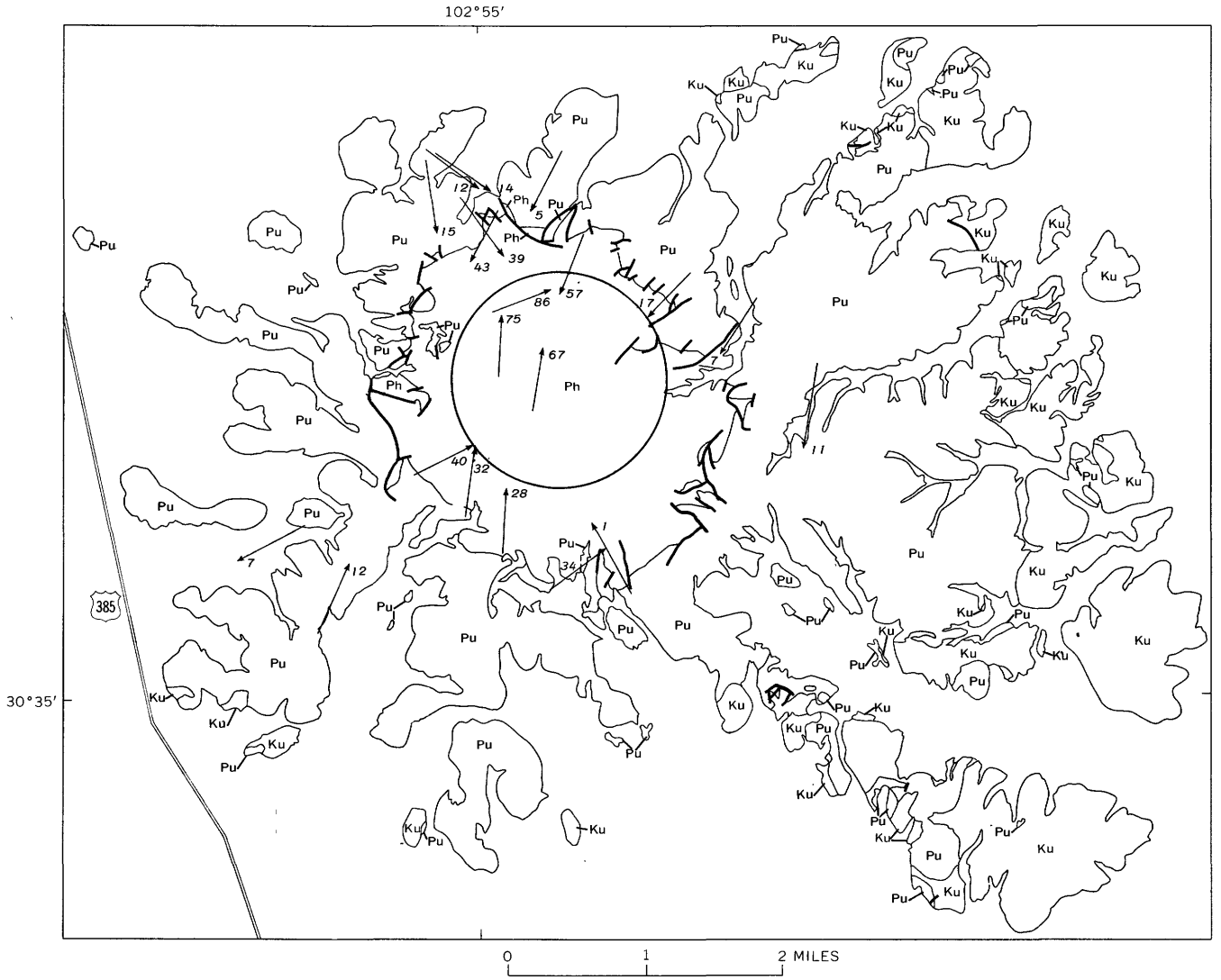

EXPLANATION

Ku

Cretaceous rocks undivided

Pu

Permian rocks undivided, exclusive of Hess Formation

Ph

Hess Formation

50

Shatter-cone axis

Arrow shows direction of point of cone, number shows angle of cone axis to horizontal after beds were rotated to horizontal

FIGURE 30.—Orientation of shatter cones in beds restored to horizontal. Circle indicates standard deviation of central focus at the top of Permian section.

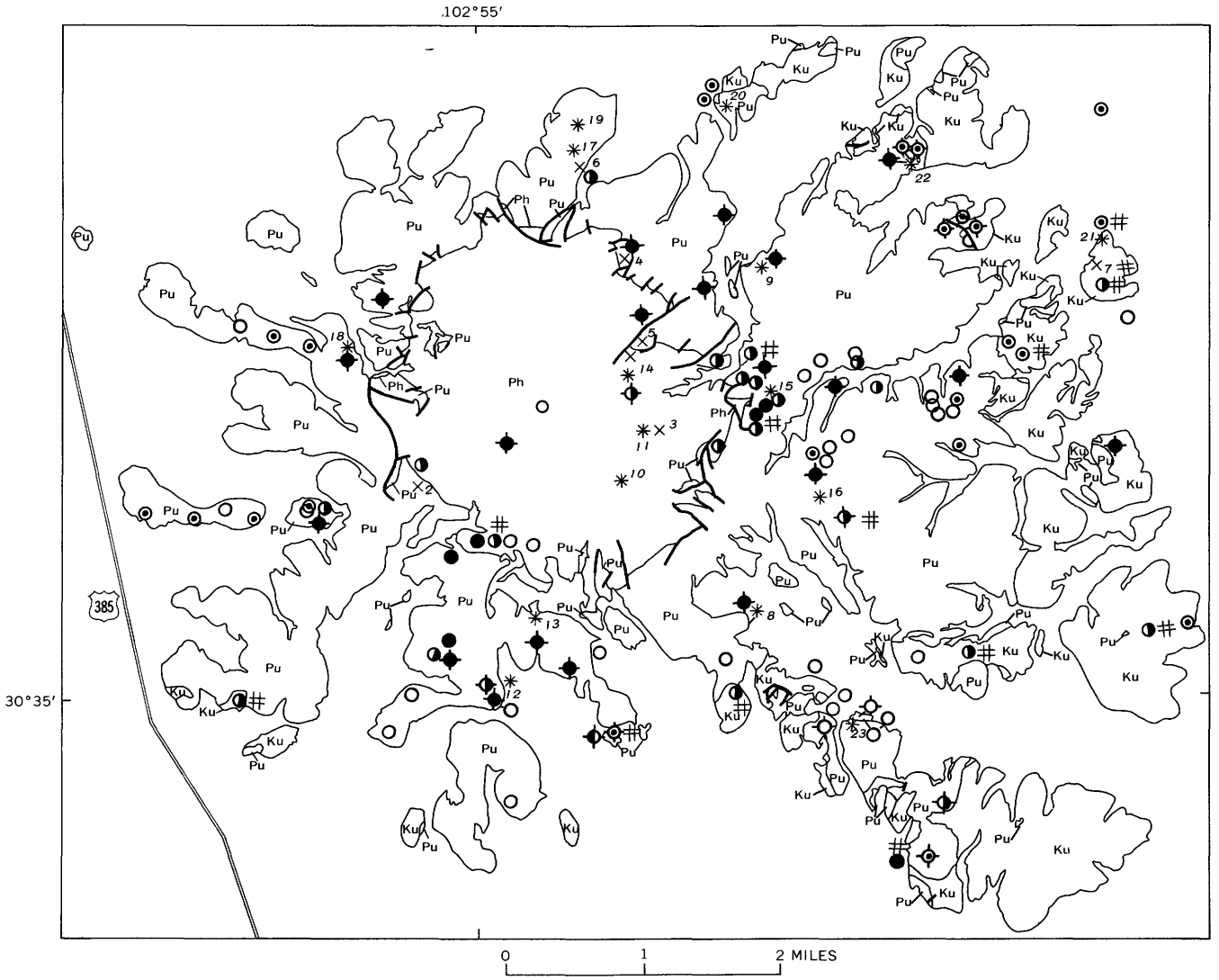

EXPLANATION

Ku — Cretaceous rocks undivided

Pu — Permian rocks undivided, exclusive of Hess Formation

Ph — Hess Formation as used by King (1930)

Relative abundance of planar structures in quartz shown by following symbols:

○ Rare or absent

◉ Present in 10-20 percent of quartz

◑ Present in 20-50 percent of quartz

● Present in more than 50 percent of quartz

Cleavage is dominant planar structure

\+ Sample from mixed breccia

×10 Planar structures measured (keyed to table 4)

FIGURE 31.—Distribution of shock-deformed quartz; degree of shock deformation is a qualitative estimate, based on flat stage microscopic examination, of the frequency of deformed grains per thin section.

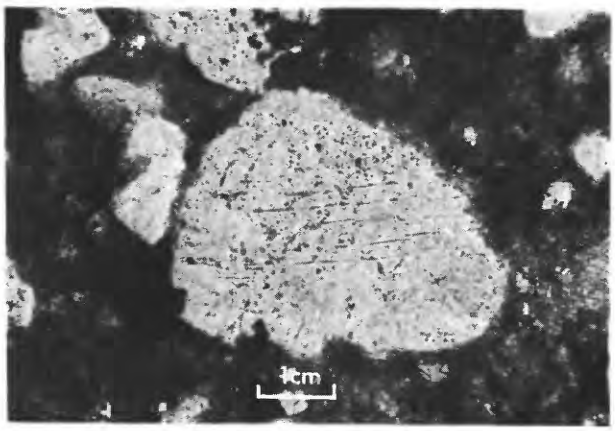

FIGURE 32.—Photomicrograph of well-developed basal cleavage (wide-spaced lines nearly east-west across grain) in quartz. Other planar elements present but not well developed. Sample is from a small pod of basal Cretaceous sandstone injected into Edwards Limestone.

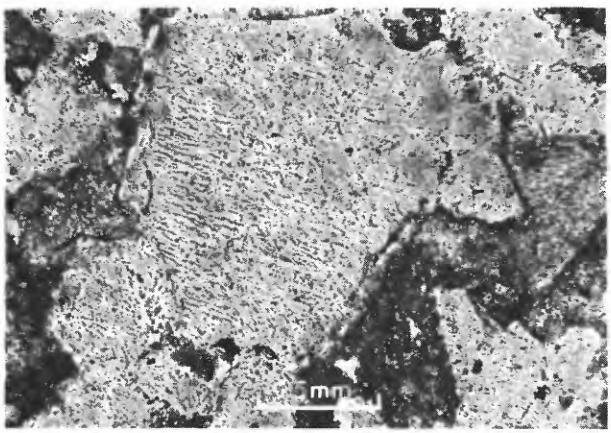

FIGURE 33.—Photomicrograph of multiple sets of planar elements in quartz. Sample is a clast of Cathedral Mountain Formation in mixed breccia.

ined several hundred thin sections of rocks from Sierra Madera and from the same formations in the Glass Mountains to determine the distribution of this type of deformation. About 1,400 sets of planar elements and cleavages were measured with a universal stage microscope in 165 quartz grains from 23 localities at Sierra Madera (fig. 31). Asterism and refractive indices of selected quartz grains were also studied. Although calcite and dolomite are also severely deformed in many rocks from Sierra Madera, they were not studied in detail.

Some types of internal structures in quartz, briefly described in table 2, were found in rocks from the Glass Mountains and presumably formed before the Sierra Madera structure. Planar elements in quartz of undeformed sandstones and conglomerates are rare, but as many as five sets in a single grain were observed. Commonly the best developed set consists of subparallel, slightly wavy discontinuities that are very difficult to bring to a recognizably vertical position on the universal stage. Other planar elements in quartz of the undeformed rocks consist of concentrations of cavities(?) that are not visibly connected. Still other planar elements, and possibly the most abundant, in quartz of unshocked rocks are not optically distinguishable, either in bright-field or phase-contrast illumination, from the shock-produced planar elements. However, unlike shock-produced elements, they tend to be widely spaced and vary greatly in length. The angular separation of such planes from the *c* axis is random, in contrast to concentrations of basal pinacoidal and rhombohedral planes among the shock-produced planar elements. Another feature, common in unshocked quartzite pebbles but not observed in densely packed quartz of shocked rocks, is planar elements that cross grain boundaries. Such planar structures are apparently irrational. The technique used by Hörz (1968, p. 249) for indexing planar elements was used and consists of matching, by rotation about the *c* axis, the largest number of poles of planar elements with a plot of poles of rational crystallographic planes in quartz. This technique gives no guarantee that an indexed plane is in fact rational; but where several planes of a particular zone can be indexed, the indication of rational crystallographic direction is strong. Using this procedure for planar structures that cross grain boundaries, it was found that in one example a planar element could be indexed as a rational crystallographic direction in one grain but not in the adjacent grain; in a second example, the planar element could not be indexed in either grain, and its angular separation from the *c* axis was quite different in the two grains.

In rocks containing the most strongly deformed quartz at Sierra Madera, virtually all quartz grains typically show multiple sets of planar elements, in marked contrast with the rarity of deformed grains in the corresponding unshocked rocks. However, gradations exist at Sierra Madera between rocks that display extensive shock damage and rocks that do not differ from their counterparts in the Glass Mountains. A qualitative estimate of the degree of shock deformation, based on flat-stage microscopic examination of the frequency of deformed quartz grains within single thin sections, is shown in figure 31. A significant feature of the distribution of shock-deformed quartz is that quartz in mixed breccias consistently shows extensive shock damage, whereas quartz in rocks still in place generally shows less shock damage and the occurrence is sporadic. Cleavages, locally the most prominent structure in quartz, are widely spaced

(about 10μ to 50μ), broad, apparently open cracks that are commonly decorated by cavities or inclusions. Although they extend to edges of grains, they do not offset grain boundaries. The most prominent set of cleavages is generally parallel to the basal pinacoid, but rhombohedral and prismatic cleavages are moderately developed (table 4). A few grains in which cleavage is subordinate to other planar elements have both basal cleavage and basal planar elements.

Examination of the planar elements with a flat stage and both bright-field and phase-contrast illumination did not allow distinction of "planar features" and "deformation lamellae" (Carter, 1968) because they are so commonly decorated by inclusions and cavities. Among the less decorated planar elements, some that are oriented at a high angle to the plane of the thin section show the asymmetric light and dark edges mentioned by Carter (1968, p. 467) as characteristic of deformation lamellae. The planar elements consist of thin, closely spaced (about 1μ to 5μ) discontinuities that are equally visible in plane- and cross-polarized light. They do not offset or cross grain boundaries. Typically there are at least five planes in a single set; such sets may occur in a single, small zone in a quartz grain, in several small zones or may be equally distributed across the entire grain. Decoration by minute cavities and inclusions is very common, but also common are such irregularities as decoration of only some planes in a single set, decoration of all planes in only one set and none in another set in the same grain, and lateral changes in degree of decoration along a single plane.

The orientation of planar elements with respect to the *c* axis of the host grain was measured in 165 grains from 23 localities at Sierra Madera (fig. 31). After measurement of each grain and appropriate rotations, an attempt was made to index the planes by a best fit to a plot of poles of rational crystallographic directions in quartz (fig. 34); by accepting measured poles that plot within 5° of the poles to rational planes, 73 percent of the planar elements were indexed, and, because several members of specific zones are consistently present, most of the indexed planes are believed to be rational. The frequency of occurrence of planar elements and cleavages is shown in figure 35, but it must be emphasized that these results are biased: grains in which the *c* axis is inclined at a low angle to the plane of the thin section were specifically selected for measurement so that basal planar elements would not be missed. However, because of the blind area of the universal stage, this meant that certain other orientations, such as some rhombohedra and prisms, could not be seen. On the other hand, when two or more members of a zone were plotted by best fit, other members of the same zone were then specifically sought; such planar elements, missed in the initial measurements because of high tilts or because their traces were nearly parallel to another set, were found in a number of cases. Apparently irrational planes were not similarly sought. Although no basal planar elements were missed, this orientation is underweighted on the histogram because for each grain there is only one such orientation, whereas the other common rational directions occur in zones of six members.

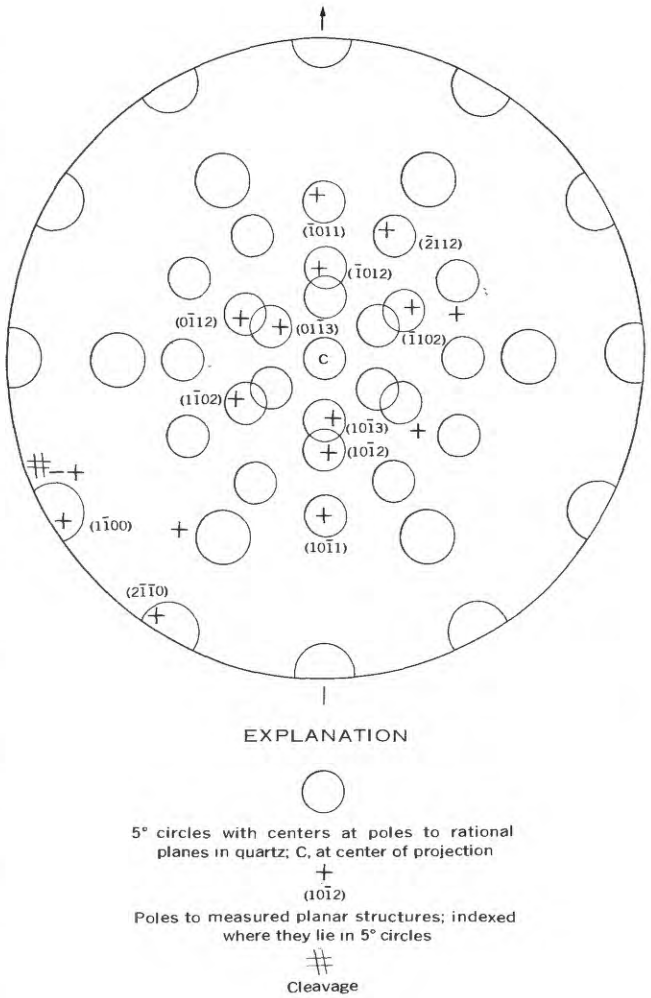

FIGURE 34.—Rotated stereogram showing best fit of measured poles (+) to sets of planar elements with poles (at center of 5° circles) to rational planes in quartz from mixed breccia.

Table 4 shows, in order of decreasing relative abundance, the most prominent rational planar elements measured in grains from the 23 localities. The number of basal orientations measured was multiplied by six to determine the position of {0001} in the table, but the number of other crystallographic orientations was not modified to account for inaccessibility or absence of some members of the zone in each grain. Accordingly,

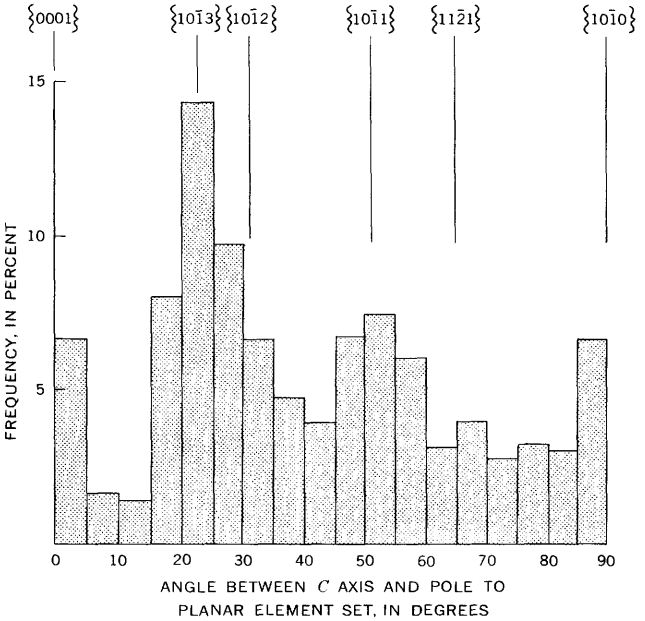

FIGURE 35.—Histogram showing frequency of all sets of planar elements measured in quartz, with respect to the angle between the *c* axis and the pole to the planar elements. Measurements of 1408 planes in 165 grains. See text for description of bias.

TABLE 4.—*Dominant planar elements in shock-deformed quartz*

Sample No.[1] and formation	Orientation of main planar elements	Number measured	Number of grains	Maximum number of well-developed sets per grain
Rocks in place				
Cathedral Mountain Formation:				
1	{0001}	9	9	8
	{10$\bar{1}$3}	14		
	{10$\bar{1}$2}	9		
	{11$\bar{2}$1}	6		
2	{0001}	5	5	3
	{10$\bar{1}$3}	5		
	{10$\bar{1}$2}	4		
	{10$\bar{1}$1}	4		
3	{0001}	9	9	8
	{10$\bar{1}$3}	21		
	{10$\bar{1}$1}	10		
	{10$\bar{1}$2}	4		
Sandstone member, Word Formation:				
4	{0001}	8	9	10
	{10$\bar{1}$3}	23		
	{10$\bar{1}$1}	8		
	{10$\bar{1}$2}	4		
5	{0001}	8	10	9
	{10$\bar{1}$3}	16		
	{10$\bar{1}$1}	11		
	{10$\bar{1}$2}	7		
Gilliam Limestone:				
6	{10$\bar{1}$3}	23	7	5
	{0001}	2		
	{11$\bar{2}$1}	5		
	{11$\bar{2}$2}	5		

See footnotes at end of table.

TABLE 4.—*Dominant planar elements in shock-deformed quartz*—Continued

Sample No.[1] and formation	Orientation of main planar elements	Number measured	Number of grains	Maximum number of well-developed sets per grain
Rocks in place—Continued				
Basal Cretaceous sandstone:				
7	[2] {0001}	6	7	13
	[2] {11$\bar{2}$1}	8		
	[2] {10$\bar{1}$1}	6		
	[2] {10$\bar{1}$0}	4		
Samples from mixed breccias				
Cathedral Mountain Formation:				
8	{10$\bar{1}$2}	23	5	17
	{10$\bar{1}$3}	16		
	{10$\bar{1}$1}	12		
	{0001}	2		
9	{0001}	8	10	9
	{10$\bar{1}$3}	17		
	{11$\bar{2}$2}	9		
	{10$\bar{1}$2}	6		
10	{0001}	4	6	7
	{10$\bar{1}$3}	23		
	{10$\bar{1}$1}	3		
11	{10$\bar{1}$3}	15	5	8
	{10$\bar{1}$2}	10		
	{10$\bar{1}$1}	4		
12	{0001}	3	5	6
	{10$\bar{1}$2}	5		
	{10$\bar{1}$3}	4		
	{10$\bar{1}$0}	4		
13	{10$\bar{1}$3}	26	6	10
	{0001}	4		
	{10$\bar{1}$2}	9		
	{10$\bar{1}$1}	6		
14	{0001}	4	5	11
	{10$\bar{1}$3}	17		
	{10$\bar{1}$2}	8		
	{10$\bar{1}$1}	6		
Sandstone member, Word Formation:				
15	{10$\bar{1}$2}	11	7	3
	{0001}	1		
	{10$\bar{1}$3}	5		
Gilliam Limestone:				
16	{10$\bar{1}$3}	15	6	7
	{10$\bar{1}$2}	2		
	{11$\bar{2}$0}	2		
17	{10$\bar{1}$3}	23	8	9
	{10$\bar{1}$2}	22		
	{10$\bar{1}$1}	4		
18	{0001}	3	5	8
	{10$\bar{1}$3}	8		
	{10$\bar{1}$2}	5		
19	{10$\bar{1}$2}	19	9	10
	{10$\bar{1}$3}	18		
	{0001}	3		
	{10$\bar{1}$1}	7		
Basal Cretaceous sandstone:				
20	{0001}	3	9	6
	{10$\bar{1}$3}	12		
	{10$\bar{1}$1}	5		
	{10$\bar{1}$0}	5		

See footnotes at end of table.

TABLE 4.—*Dominant planar elements in shock-deformed quartz*—Continued

Sample No.[1] and formation	Orientation of main planar elements	Number measured	Number of grains	Maximum number of well-developed sets per grain
Samples from mixed breccias—Continued				
Basal Cretaceous sandstone—Continued				
21	{0001}	8	9	8
	{10$\bar{1}$1}	14		
	{10$\bar{1}$3}	13		
	{11$\bar{2}$2}	12		
	{10$\bar{1}$2}	7		
22	{0001}	6	8	11
	{10$\bar{1}$3}	20		
	{10$\bar{1}$2}	12		
	{10$\bar{1}$1}	6		
23	{0001}	5	6	7
	{10$\bar{1}$3}	7		
	{10$\bar{1}$1}	6		

[1] Keyed to fig. 34.
[2] Cleavage is dominant.
Note.—The relative abundance of {0001} takes into consideration that there is only one such orientation compared to a possible six members of other zones.

table 4 gives only a qualitative picture of the relative abundance of the different planar elements. Despite the statistical flaws, it is apparent that the dominant orientations of planar elements are parallel to {0001}, {10$\bar{1}$3}, {10$\bar{1}$1}, {10$\bar{1}$2}, and {10$\bar{1}$0} at the 23 localities. Studies by Carter (1965, 1968), Chao (1967b), and Short (1966a) have demonstrated that both the multiplicity [1] and the common orientations of these planar elements are grossly unlike those developed in tectonites at slow strain rates, and that they are the same as those formed by shock, both naturally (Bunch and Cohen, 1964; Engelhart and Stöffler, 1965; Chao, 1967a, b; and other workers) and experimentally (Short, 1965, 1966a, b, 1968a, b; Hörz, 1968; Müller and Défourneaux, 1968; and Bunch and others, 1968).

In experiments performed by Hörz (1968), single quartz crystals shock loaded at pressures of about 50 kb (kilobars) and higher developed cleavages oriented like those at Sierra Madera. Hörz' experiments showed that basal and prismatic cleavages form when the impact direction is normal to {10$\bar{1}$1} and that unit rhombohedral cleavages form when impact is normal to {0001} and {10$\bar{1}$0}. Planar elements form in single quartz crystals only at pressures of over 100 kb (Hörz, 1968; Müller and Défourneaux, 1968), but the orientations of the planes are independent of the impact direction. Müller and Défourneaux (1968) reported formation of planar features parallel to {10$\bar{1}$3} at shock pressures above 105 kb; Hörz (1968) reported their formation at pressures above 119 kb. Planar features parallel to {10$\bar{1}$2} first formed between 160 and 200 kb in Hörz' experiments and above 200 kb in experiments by Müller and Défourneaux. Above 250 kb, planar features parallel to {10$\bar{1}$2} are about as common as those parallel to {10$\bar{1}$3} (Hörz, 1968).

The data from measured samples and from flat-stage examination indicate that cleavages are best developed in quartz from rocks that are far from the center of Sierra Madera or from less strongly deformed rocks closer to the center. Of the measured planar elements, {10$\bar{1}$3} is dominant over {10$\bar{1}$2} in all samples of Cretaceous rocks, whether in place or in mixed breccia, and in the majority of Gilliam fragments in mixed breccia; {10$\bar{1}$2} is as well or better developed than {10$\bar{1}$3} in samples of Word and older rocks from mixed breccia. These relations indicate that, in general, rocks closer to the center of the structure record the highest pressures and those incorporated in mixed breccias were subjected to higher pressures than equivalent rocks that remained in place. Experimental data referred to above suggest that rocks incorporated in mixed breccias were subjected to pressures in excess of about 200 kb near the center of the structure, rocks still in place near the center were locally subjected to pressures above about 100 kb, and those around the edge of the central uplift were subjected to pressures of about 50 kb and higher. Although these pressures are believed to be of the right order of magnitude and are compatible with those suggested by Robertson and others (1968) for the same types of deformation, experimental data from single quartz crystals probably cannot be extrapolated directly to sandstones. Kieffer's (1969) theoretical treatment of shock-wave propagation through granular quartz (Rinehart, 1968; Chao, 1968) suggests that a considerable range of peak pressures could be recorded in different but nearby grains of a sandstone because reverberation of shock and rarefaction waves created by multiple grain impacts results in local energy concentrations not produced in similar solid material. Accordingly, an accurate appraisal of peak pressures reached at different points on Sierra Madera would require a considerably more sophisticated study of the shock deformation.

In addition to the planar elements in quartz at Sierra Madera, permanent crystal damage is indicated by pronounced asterism (see Dachille and others, 1968) and abnormal refractive indices of deformed grains. Asterism—spreading of spot reflections from single grains X-rayed during rotation in a Debye-Scherrer camera—is apparent in photographs of shocked quartz and calcite shown in figure 36. Photographs of unshocked calcite and quartz (Nos. 2 and 4) are shown for comparison. A quartz grain from the basal Cretaceous sandstone in the Glass Mountains, chosen to show

[1] The maximum number of planar element sets measured in a single quartz grain from Sierra Madera is 22, of which 14 were matched to rational directions by best fit.

that slight asterism may also be displayed by unshocked minerals. The undulose extinction of this grain indicates that asterism was produced by strain. In Sierra Madera samples, asterism ranges from slight in weakly deformed grains to patterns approaching those expected from powder mounts. Different degrees of asterism for different grains from the same sample are characteristic. The degree of asterism illustrated for quartz samples as a whole is roughly correlative with the departure of the refractive index n_O from its normal value of 1.544; thus, samples 192 and 143, which show the most marked asterism, have the lowest value of n_O. Samples 186, 159, and 112 show less abnormal refractive indices and less asterism; they also show a greater range of refractive index and asterism. The range of refractive index ($n_O = 1.538–1.544$) and asterism also correlates with the degree of shock damage inferred from the orientations and relative abundances of planar elements. Thus, samples 192 and 143 are from mixed breccias in which planar elements indicate high shock pressures, sample 112 is from the Cathedral Mountain Formation in place in which moderate shock pressures are indicated, and samples 186 and 159 are from slightly shocked Cretaceous sandstone in mixed breccias on the flanks of the central uplift. Reduced refractive index and extreme asterism shown by the severely deformed quartz suggest pressures above about 200 kb. (See Hörz, 1968; Chao, 1968.)

Coesite and stishovite reflections were looked for in all the X-ray photographs, but none were found. A few other highly shocked samples were searched, also unsuccessfully, for these high-pressure silica polymorphs, but special techniques for concentration were not employed.

SUMMARY OF SHOCK DEFORMATION

Four main products of shock deformation are found at Sierra Madera: monolithologic breccias, mixed breccias, shatter cones, and deformed quartz and carbonate minerals. The general absence of shock-deformed quartz in monolithologic breccias and scattered occurrences of deformed calcite and dolomite in these breccias and in shatter-coned rocks suggest that monolithologic breccias and shatter cones formed at comparatively low pressures. All rocks emplaced as mixed breccias in Gilliam and older strata contain quartz that has been severely deformed at peak pressures of over 200 kb, whereas rocks still in place contain quartz that was subjected to pressures from about 50 kb, at the flanks of the uplift, to more than 100 kb, nearer the center of the structure. Considerably higher pressures may have accompanied shock melting of certain clasts in a centrally located mixed breccia.

The shock predated the central uplift, as shown by the rotations of shatter cones. Ideally the shock wave might be considered to have propagated as an expanding hemisphere from the approximate focus indicated by shatter cones. Shock intensity should have decreased with increasing radius of the hemisphere. After uplift, the presently exposed Hess Formation should all have been about equidistant initially from the shock origin; but outward the exposed Gilliam Limestone should have been half again as far from the shock origin, and the nearest exposed Cretaceous strata, more than twice as far as the lowest exposed Hess beds. In a crude way this is consistent with the gross distribution of shock deformation features.

ORIGIN

The keys to the origin of Sierra Madera are: (1) lack of relationship to local and regional structure, (2) the shape of the deformed zone, in which intensity of deformation diminishes laterally and downward from the center, (3) geometry of the central uplift, which closely restricts the choices for its mode of formation, and (4) shock deformation features that indicate peak pressures in excess of 200 kb and a shock source located above the center of the structure. Although certain of these features are compatible with a terrestrial origin, taken together they can be viewed only as evidence of deformation resulting from a surface impact event.

REGIONAL AND LOCAL SETTING

The Sierra Madera structure is unique in its form, style, and severity of deformation in a broad region of otherwise mildly deformed rocks of Permian and Early Cretaceous age. The structure formed some time after the Lower Cretaceous strata were deposited but probably before they were completely consolidated, thus, in Late Cretaceous or early Tertiary time. During that time the region, including the Delaware and Val Verde basins, was apparently undergoing only very mild deformation. Major late Cenozoic block faults occur in some parts of the Delaware basin (King, 1948) but only in areas remote from Sierra Madera. Although Sierra Madera is unique in this region, its general setting—a moderate thickness of shelf-facies sedimentary rocks overlying a thick section of basin-facies rocks—is common around the Permian basins (fig. 3; Oriel and others, 1967).

Sierra Madera is near the northeast end of the Glass Mountains, a gently north-dipping homocline of Permian and Lower Cretaceous strata. The main structural features of the Glass Mountains—northwest tilting and minor folding into low domes and north-trending anticlines—formed before deposition of the Lower Cretaceous rocks (King, 1930, p. 127). Lower Creta-

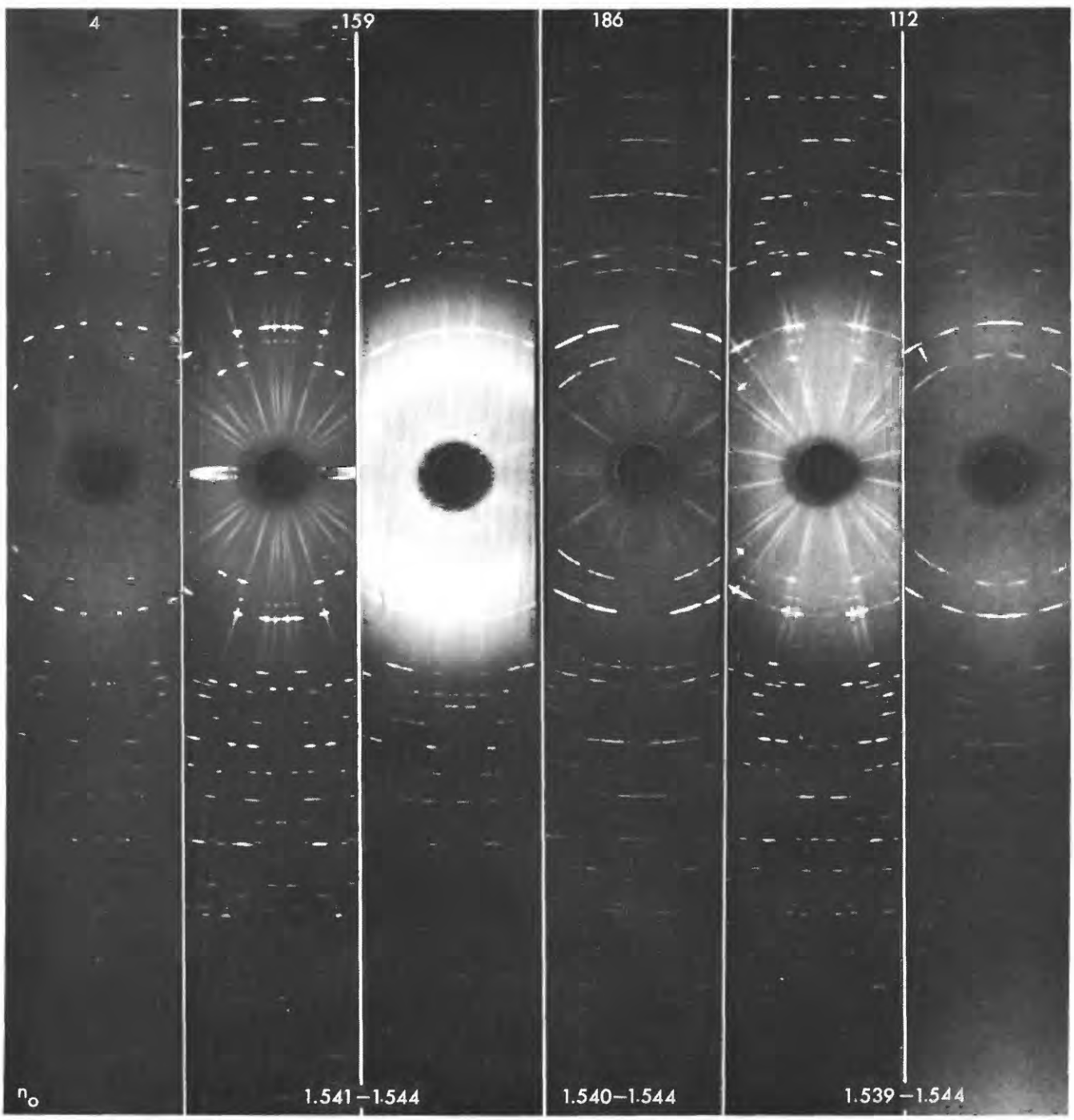

FIGURE 36.—Debye-Scherrer X-ray photographs of shocked quartz and calcite showing asterism, and of the unshocked minerals for comparison. Refractive index (n_o) of quartz determined on crushed grain mounts. Pairs of photographs of the same sample show extremes of asterism of different grains from a single specimen, and the range of n_o represents the samples as a whole. No. 4 is unshocked quartz from the basal Cretaceous sandstone in the Glass Mountains. No. 2 is unshocked calcite from the

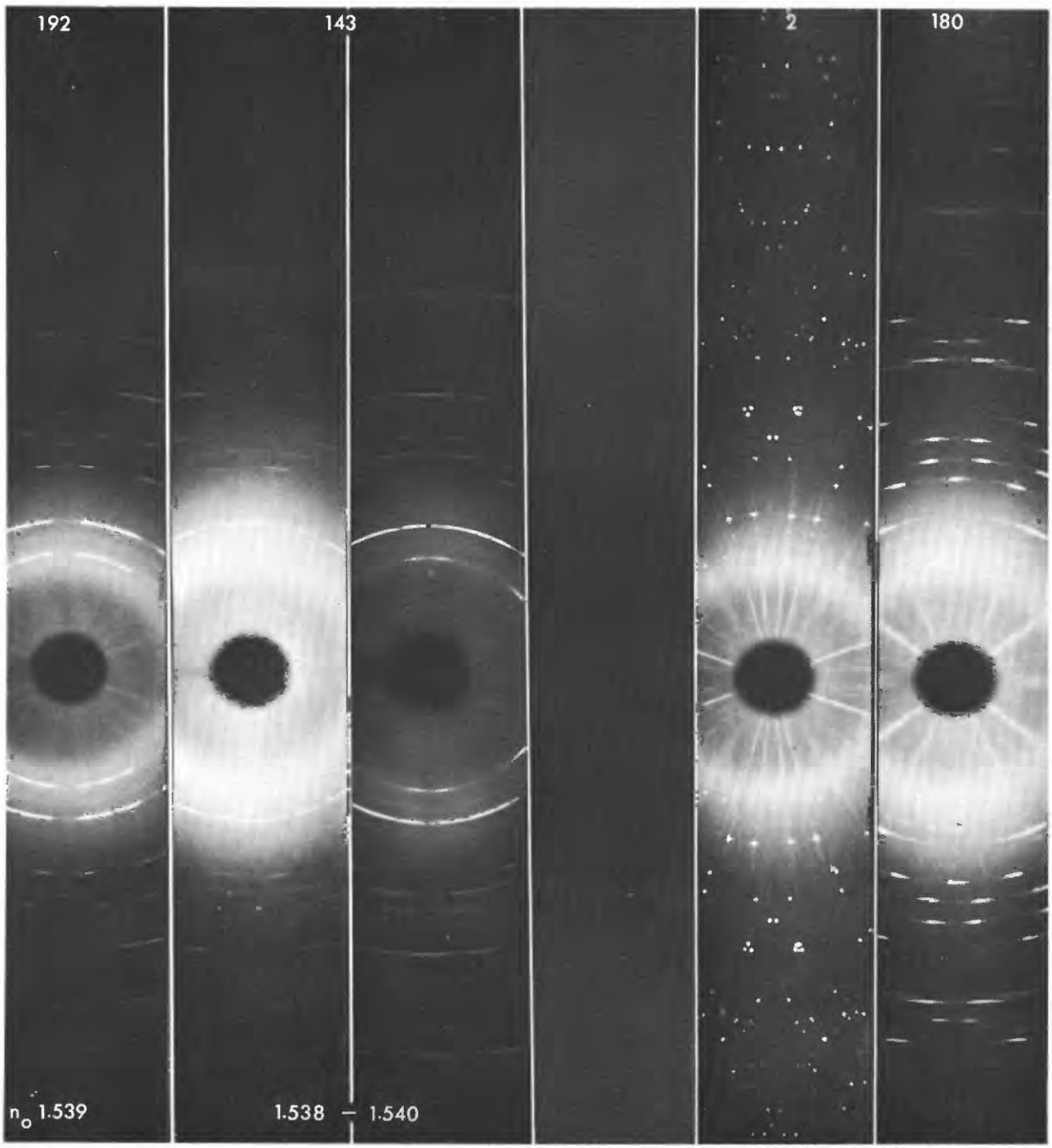

Vidrio Member of the Word Formation in the Glass Mountains. Nos. 159, 186, 112, 192, and 143 are shocked quartz, and No. 180 is shocked calcite from Sierra Madera. The second photograph of No. 143 has the two strongest reflections of an iron-rich chlorite that forms inclusions along the planar elements.

ceous strata were deposited on the beveled surface of Permian rocks, and the strata were later (probably near the close of the Pliocene) retilted and broken by a system of northwest-trending normal faults (King, 1930, p. 127), few of which intersect the Sierra Madera structure. Hence, the very mild deformations of the Glass Mountains appear to have bracketed the formation of Sierra Madera. A fault, possibly Tertiary in age, has about 400 feet of displacement in Lower Cretaceous rocks (pl. 1, near Hunt Elsinore 31) north of Sierra Madera but does not intersect the structure. Sierra Madera lies above the north flank of an east-west trending subsurface anticline. (See fig. 6, Hunt Elsinore 52 and 53.) The fold must have formed before Permian time because Pennsylvanian strata were eroded from its top and rocks of Permian age and younger are not affected by it.

Zimmermann and Amstutz (1965, p. 304) and Lowman (1965) have suggested, respectively, that Sierra Madera is part of a regional lineament and that it is a member of a regional association of features. Zimmermann and Amstutz implied that Sierra Madera is alined with the Solitario dome and breccia pipes in the Terlingua district, and Lowman considered it to be part of the Trans-Pecos Tertiary igneous province. However, Sierra Madera is not connected with these features by any structure expressed in rocks exposed at the surface or known to exist in the subsurface, and moreover, it is very different from all these other features.

Because Sierra Madera is unique in an otherwise common regional setting and because it is not connected either spatially or in time with local structures, we conclude that the cause of deformation is not genetically related to regional or local features.

ZONE OF DEFORMATION

Surface mapping and drill data indicate that the intensity of folding and faulting dies out rapidly from the center of Sierra Madera, both laterally and downward. Hence, the gross shape of the zone of deformation is that of a cup or funnel about 8 miles in diameter and 6,000 to 8,000 feet deep, with the most intensely deformed rocks in the upper central part. The intense shattering of rocks seen at the surface similarly disappears downward and was not observed in cuttings from the Phillips well at depths greater than about 2,800 feet (Eggleton and Shoemaker, 1961). The shape of the zone of deformation as well as the distribution of the more severely disrupted rocks accordingly indicates that the deforming forces originated high in the affected section of rocks and near the center of the structure.

GEOMETRY OF THE CENTRAL UPLIFT

Formation of the central uplift involved both radial inflow and uplift of strata. This structural pattern leads to the conclusion (Wilshire and Howard, 1968) that the uplift could not have formed by a doming process involving (1) emplacement of material, such as magma (King, 1930; Lowman, 1965), (2) diapiric intrusions of salt or shale (Lowman, 1965), or (3) solid blocks of subjacent strata or basement rock (Amstutz, 1960), beneath the uplifted rocks. All such mechanisms would require distension of the section rather than the observed compression. Igneous intrusions, saline diapirs, and reactivated basement structures are also disproved by drill data. Centripetal movement of strata in the uplift furthermore rules out an explosion at depth (Milton and Brett, 1968), perhaps the most prominent hypothesis for the terrestrial origin of cryptoexplosion structures (Bucher, 1963; Snyder and Gerdemann, 1965).

Structures of terrestrial origin that do resemble the central uplift of Sierra Madera are diapirs, and a diapiric origin for cryptoexplosion structures has been proposed by Amstutz (1964) and Zimmermann and Amstutz (1965). The form of the uplift at Sierra Madera resembles that within diapiric structures such as salt domes, so that any explanation by diapirism must seek the motivating cause within the section of rocks now exposed. The only appropriate density contrast for initiating buoyant diapirism is between the dominantly shaly lower Hess and older Permian strata and the overlying, dominantly carbonate rocks of upper Hess and younger rocks. An origin of the uplift by emplacement of a shale diapir yet unexposed runs into the same geometrical problem as formation by other intrusions, namely, the addition of new material, which would cause outward rather than inward movement. Despite the resemblance of the uplift and ring depression to salt domes, notable differences at Sierra Madera include the structurally high rim containing upward-driven slices of older rocks and the various signs of shock deformation, not known in any bonafide diapiric structure. Hence, an origin by diapirism is untenable.

Several hypotheses have been advanced for the origin of central uplifts in impact craters, such as reflection of shock waves from deep discontinuities (Dence and others, 1965), isostatic adjustment (Dence and others, 1965), and elastic rebound (Rooke and Chew, 1965). None of these, however, account for the radial inflow of rock responsible for the structural geometry of the uplifts; other strong objections have also been lodged against these mechanisms (Beals, 1965; Dence, 1968).

Uplifts with a geometry apparently similar to that of Sierra Madera have been produced in high-explosive cratering experiments [2] performed in Canada (Diehl

[2] The analogies in cratering mechanics of impacts and explosives were discussed by Shoemaker (1960). An excellent recent paper by Moore (1969) points out the similarities in subcrater deformation between craters produced by missile impact and by explosives.

and Jones, 1967; Roddy, 1968b) where the charge was detonated at ground surface rather than buried beneath it. Roddy (1968a, b; 1969b) likened this surface detonation of explosives to the low penetration capacity of an impacting comet, as opposed to an iron or stony meteorite, and suggested that craters with uplifts were produced by the impact of comets. Experimental impact of low-density projectiles with metals and water (for example, Partridge and Van Fleet, 1959; Engel, 1962; Worthington, 1963; Harlow and Shannon, 1967b) have also produced central uplifts, but the mechanics of uplift have not yet been fully explained. Dence (1968) suggested that collapse of crater walls along inward-dipping shear surfaces that extend below the crater could produce the observed geometry of the uplifts. We have no information that allows a choice between these proposals. In any case, the occurrence of uplifts in impact craters is apparently related to the scale of the event—most known and suspected terrestrial impact structures more than 1½–2 miles wide contain central uplifts and smaller ones do not. On the moon, where gravity is one-sixth that on earth, craters with central peaks are generally more than 12 miles wide.

SHOCK DEFORMATION

Two types of deformation common at Sierra Madera—shatter cones and, especially, internal structures in quartz—appear to have well-substantiated shock-wave origins. The symmetry of shatter cone orientations indicates that shock waves were generated at a central focus in the structure and at a level high in the section of deformed rocks; the shock wave passed downward and outward from this focus at a time when the strata were nearly flat lying. Local peak pressures reached during passage of the shock wave were in excess of 200 kb in rocks incorporated in mixed breccia masses. Peak pressures recorded in quartz of rocks still in place are crudely zoned (fig. 31), such that older rocks near the center of the structure were subjected to pressures in excess of about 100 kb and those on the periphery of the uplift were subjected to pressures on the order of 50 kb. This crude zoning is comparable to what might be expected from deformation, uplift, and erosion of the generalized subcrater shock zones described by Dence (1968, p. 179).

CONCLUSIONS ON ORIGIN

Of the four significant features of Sierra Madera that bear on its origin, two—the shape of the deformed zone and shock deformation—clearly indicate an origin by surface impact. One of the remaining two—lack of relationship to local structure—is consistent with an impact hypothesis. The fourth feature—geometry of the central uplift—was discussed mainly in terms of its inconsistency with other proposed mechanisms of uplift in cryptoexplosion structures. Although the mechanics of uplift have not yet been fully explained, the existence of such uplifts in craters of probable impact origin has been established (Roddy, 1968a; Engelhart and others, 1967).

DEPTH OF EROSION

Bucher (1936) recognized the structural characteristics of cryptoexplosion structures. Other features, such as shatter cones and shock deformation of minerals, have also been shown to be characteristic of such structures. (See Short and Bunch, 1968). Because these structures formed at different times, ranging from Precambrian for the Vredefort ring of South Africa to Miocene for the Steinheim Basin of Germany, and because they formed under different conditions, present exposures show a wide range of erosional level. Nevertheless, their common characteristics tie them together and allow the more deeply eroded structures, such as Sierra Madera, to be reconstructed by comparison with those that are less eroded. The structures at Flynn Creek, Tenn. (Roddy, 1968a), and Steinheim Basin (Branco and Fraas, 1905; Engelhart and others, 1967) represent the highest levels of exposure in well-studied cryptoexplosion structures. Both structures have a small central uplift surrounded and partly buried by a lens of breccia that occupies a shallow crater; the crater rim at Flynn Creek has well-developed concentric folds, and a small lens of breccia ejected from the crater is preserved in a graben (Roddy, 1968a). A somewhat lower erosional level is found at Gosses Bluff, Australia (Milton and Brett, 1968), where some highly shocked and melted fallback breccia is preserved, but the original crater walls have been destroyed by erosion. Sierra Madera represents a still lower erosional level from which all vestiges of a crater-form depression, fallback, and ejecta have been stripped. We infer from the other cryptoexplosion structures that the outer rim of Sierra Madera represents folded strata beneath the original crater rim, that, before erosion, the central uplift protruded into the crater, and that the crater was comparatively shallow. Experimental craters in which analogous folds formed beneath the crater walls include the nuclear explosion crater Jangle U (Shoemaker, 1968), the chemical explosion craters Snowball and Prairie Flat (Roddy, 1968a), and certain impact craters in sand (Gault and others, 1968, fig. 18). Scaling to the approximate dimensions of the Flynn Creek crater and various experimental craters suggests that about 2,000 feet of cover may have been present over Lower Cretaceous strata and have now been removed by erosion (fig. 37).

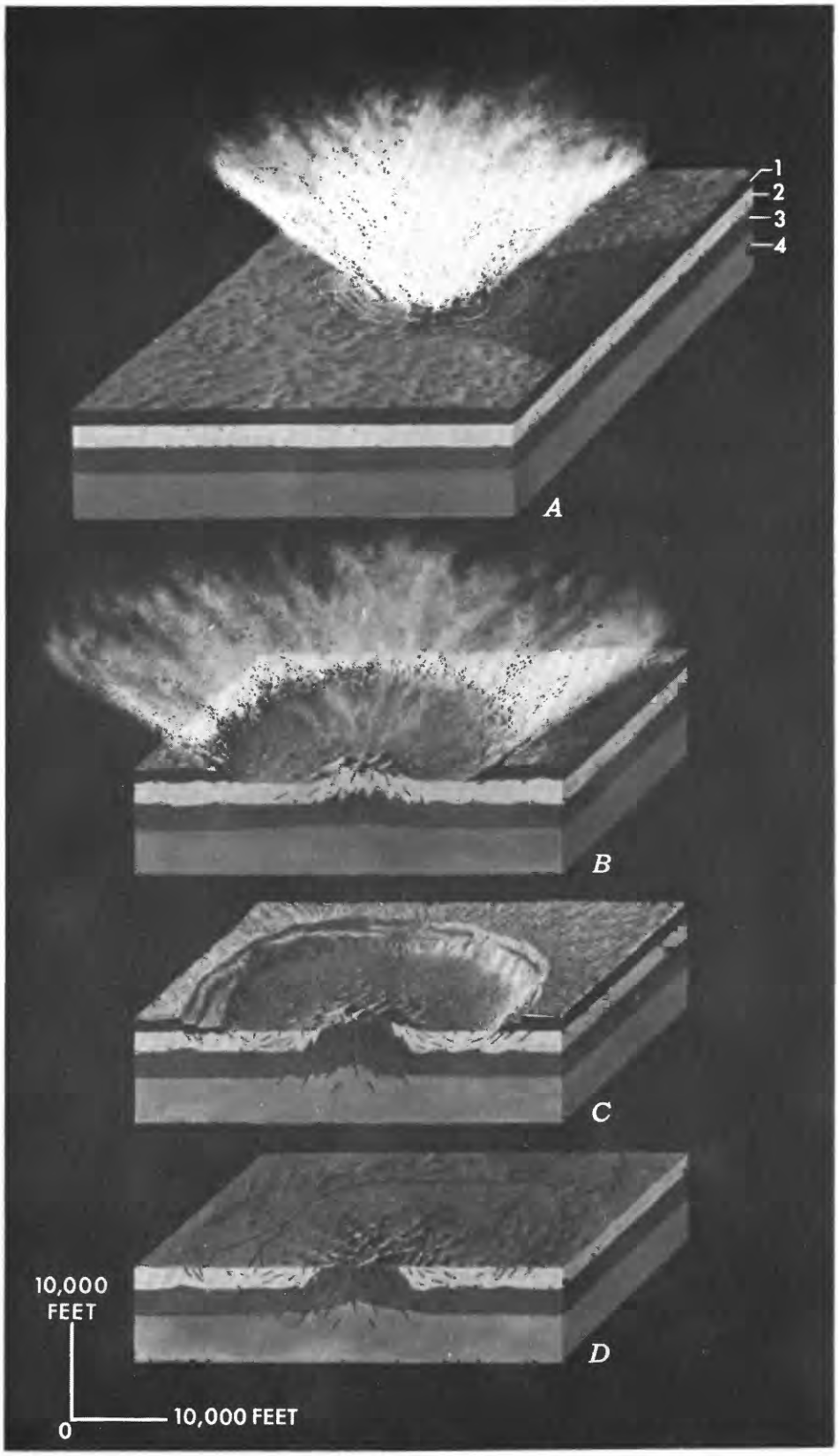

FIGURE 37

Alternatively, the Lower Cretaceous strata may have been under water.

HYPOTHETICAL RECONSTRUCTION OF THE EVENT

Figure 37 illustrates our concept of how Sierra Madera formed. Immediately after impact (fig. 37*A*), the crater grew by low-angle jetting (Gault and others, 1968), while a shock wave passed outward and downward. Figure 37*B* shows the central uplift forming during excavation of the crater, in accordance with the Canadian high-explosive cratering experiments and with the sequence inferred at Gosses Bluff (Milton and Brett, 1968). Outward thrusting may have dragged or injected slices of dolomite from the Tessey up around the periphery; the slices were then left isolated by subsequent normal faulting related to crater wall collapse. Withdrawal of material moving into the uplift may have caused collapse of the crater walls, or inward movement of collapsing wall blocks may have been responsible for the uplift. Either way, the adjustments may have continued past the excavation stage. Injection of sandstone and of highly shocked, shattered rock in mixed breccias probably began early in the deformation. If analogous to sand flows around the Snowball TNT crater (Diehl and Jones, 1967), some of the fluidized injections may have continued to flow for days. The freshly formed crater is shown complete in figure 37*C*. Figure 37*D* represents the present eroded form of the structure.

APPLICATION TO LUNAR STUDIES

Sierra Madera was studied, not only to elucidate the origin of the structure, but also to apply the results to lunar analogs. The concept that Sierra Madera formed by impact was first promulgated by Boon and Albritton (1937) and was shared by Shoemaker and Eggleton (1964), who started the current project. Understanding of the positions of the various structural elements with respect to the original crater required comparison of Sierra Madera with other structures in the same class that are less eroded (Roddy, 1968a; Milton and Brett, 1967). Perhaps the most important result of these studies for application to lunar problems is the establishment of the subcrater source of the strata composing the uplifts. These results suggest the possibility of sampling not only the thickness of lunar crust exposed in the walls of craters with central uplifts, but also of subcrater crustal material from depths approximately one-tenth of the crater diameter.

Central uplifts dominate the structure at Sierra Madera and a number of similar cryptoexplosion structures also believed to be the eroded roots of impact craters. In natural structures retaining the surficial crater, such as at Flynn Creek, Tennessee, and in the Snowball and Prairie Flat experiment craters, each of which was formed by explosion of 500 tons of TNT (Roddy, 1968a), central uplifts are expressed morphologically as central hills. Large craters in the Canadian Shield, such as East Clearwater Lake (Dence and others, 1965) and Deep Bay (Dence and others, 1968), also contain central peaks presumed to represent uplifts. Central uplifts or peaks are, in fact, recognized at most presumed astroblemes wider than a few miles. Hence, it is reasonable to expect that such uplifts are also represented by the central peaks of the impact craters on the moon.

Typical of lunar craters having central peaks is Copernicus (fig. 38), commonly considered the type example of an impact crater since Shoemaker's analysis

FIGURE 37.—Hypothetical reconstruction of events forming Sierra Madera. 1, Post-Lower Cretaceous, pre-Quaternary strata (hypothetical). 2, Lower Cretaceous, Ochoan, and Guadalupian strata. 3, Leonard strata. 4, Wolfcamp strata. *A*, shortly after impact showing growth of crater by low-angle jetting. *B*, seconds after *A*, showing crater growth by ejection and formation of overturned flap; outward directed compression forms rim folds concurrently with or followed by inward movement of strata beneath the crater beginning formation of central uplift. *C*, freshly formed crater days after impact, showing uplift protruding into crater, crater-rim modification by slumping, and fallback and ejecta mantle. *D*, present form of Sierra Madera, modified by erosion. Painting by Don Davis.

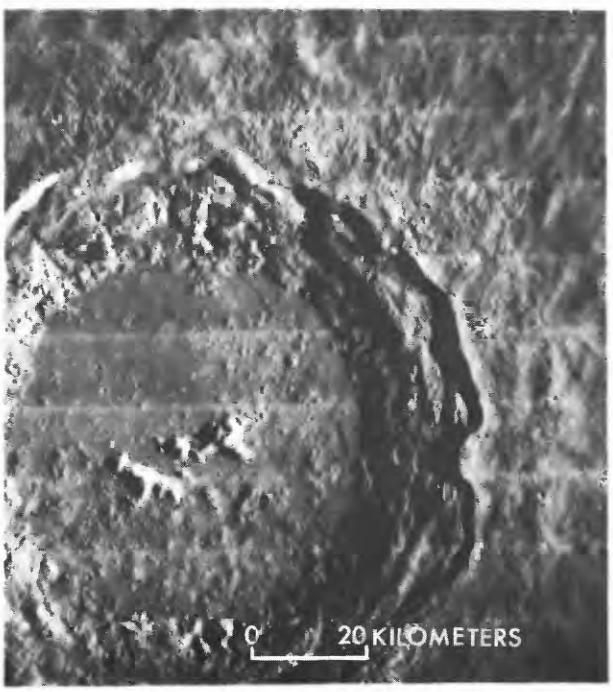

FIGURE 38.—The lunar crater Copernicus. Orbiter IV photograph, courtesy of NASA.

(1962). A survey of other lunar craters that have the characteristics expected of fresh impact craters, namely, a hummocky rim, field of secondary craters, and rays, reveals that nearly all wider than about 15 miles contain central peaks. The crater walls are characteristically slumped. The central peaks are commonly surrounded by a relatively flat floor, which may represent pooled fallback or impact melt. The peaks are situated near the center of the crater and range in shape from a cluster of hills, as in Copernicus, to massive irregular mountains, as in Theophilus or Tsiolkovsky. If truly uplifts, such central peaks expose deep-seated rocks where they can be sampled at the moon's surface.

Using Sierra Madera and similar structures as a guide, exposures of the central peaks in lunar impact craters can be expected to be in grossly concentric bands of increasingly more deep-seated rocks toward the center. The pattern will be complicated structurally by numerous folds and faults and by brecciation and shock deformation. Shatter cones, intrusion breccias, and monolithologic breccias are likely to be abundant. Intrusion breccias, in particular, may show more shock effects than nearby rocks that are still in place. If the rocks now comprising the central uplift were originally layered approximately horizontally, as at Sierra Madera, then these layers will now have steep dips for the most part and will crop out concentrically. Any evidence for such concentric layering found in future high-illumination orbital photography of fresh well-exposed central peaks would be extremely valuable both for its implications regarding crustal evolution and for specific mission planning.

An astronaut mission to the central peak area of a large impact crater such as Copernicus offers a fine opportunity to sample deep-seated lunar rocks. Ideally, such a mission would concentrate on a planned traverse into the core of the central peak area, in order to sample progressively deeper rocks along the way and describe their mode of occurrence in place. In practice, the core may be difficult to identify. Even on a mission with greatly restricted mobility, a variety of rocks could be collected by a short traverse along the base of one of the peaks, for blocks and apparent outcrops are common on the central peaks of Copernicus and some other fresh craters as well. Samples of unbrecciated rocks are likely to show the least effects of the impact and thus be most representative of the lunar subsurface.

Central peaks of larger craters should expose rocks uplifted from greater depths. The amount of uplift is about a tenth of the crater diameter at the Flynn Creek crater and the Snowball and Distant Plain 6 experimental craters (Roddy, 1968a), which were formed by explosion of 500 and 100 tons of TNT, respectively. At Sierra Madera, the 0.8 mile uplift is about 10 percent of the width of the circular deformed zone, and the ratio varies from 5 to 15 percent at a number of similar structures ranging in size from Steinheim, 2 miles across, to Vredefort, about 100 miles across. If a similar relation holds for lunar craters, then the central peak of Copernicus exposes rocks uplifted on the order of 6 miles (10 km) and the peaks of the larger craters Tsiolkovsky and Humbolt expose rocks uplifted on the order of 12 miles (20 km).

REFERENCES CITED

Adkins, W. S., 1927, The geology and mineral resources of the Fort Stockton quadrangle: Texas Univ. Bull. 2738, 166 p.

Amstutz, G. C., 1960, Polygonal and ring tectonic patterns in the Precambrian and Paleozoic of Missouri, U.S.A.: Eclogae Geol. Helvetiae, v. 52, no. 2, p. 904–913.

——— 1964, Impact, cryptoexplosion, or diapiric movements?: Kansas Acad. Sci. Trans., v. 67, no. 2, p. 343–356.

Balk, Robert, 1949, Structure of Grand Saline salt dome, Van Zandt County, Texas: Am. Assoc. Petrol. Geol. Bull., v. 33, no. 11, p. 1791–1829.

Beals, C. S., 1965, The identification of ancient craters, *in* Geological problems in lunar research: New York Acad. Sci. Annals, v. 123, art. 2, p. 904–914.

Blount, D. N., and Moore, C. H., Jr., 1969, Depositional and nondepositional carbonate breccias, Chiantla quadrangle, Guatemala: Geol. Soc. America Bull., v. 80, no. 3, p. 429–442.

Boon, J. D., and Albritton, C. C., Jr., 1936, Meteorite craters and their possible relationship to "cryptovolcanic structures": Field and Lab., v. 5, no. 1, p. 1–9.

——— 1937, Meteorite scars in ancient rocks: Field and Lab., v. 5, no. 2, p. 53–64.

Branco, W., and Fraas, E., 1905, Das kryptovulkanische Becken von Steinheim: Akad. Wiss. Berlin, Phys.-Math. K1, Abh., v. 1, p. 1–64.

Bray, J. G., and others, 1966, Shatter cones at Sudbury: Jour. Geol., v. 74, no. 2, p. 243–245.

Bucher, W. H., 1936, Cryptovolcanic structures in the United States: Internat. Geol. Cong., 16th, Washington, D.C., Rept., pt. 2, p. 1055–1084.

——— 1963, Cryptoexplosion structures caused from without or from within the Earth? ("astroblemes" or "geoblemes"?): Am. Jour. Sci., v. 261, no. 7, p. 597–649.

Bunch, T. E., and Cohen, A. J., 1964, Shock deformation of quartz from two meteorite craters: Geol. Soc. America Bull., v. 75, p. 1263–1266.

Bunch, T. E., Cohen, A. J., and Dence, M. R., 1968, Shock-induced structural disorder in plagioclase and quartz, *in* French, B. M., and Short, N. M., eds., Shock metamorphism of natural materials: Baltimore, Md., Mono Book Corp., p. 509–518.

Bunch, T. E., and Quaide, W. L., 1968, Shatter cones in the Danny Boy nuclear crater, *in* French, B. M., and Short, N. M., eds. Shock metamorphism of natural materials: Baltimore, Md., Mono Book Corp., p. 285.

Carter, N. L., 1965, Basal quartz deformation lamellae—A criterion for recognition of impactites: Am. Jour. Sci., v. 263, no. 11, p. 786–806.

Carter, N. L., 1968, Dynamic deformation of quartz, *in* French, B. M., and Short, N. M., eds., Shock metamorphism of natural materials: Baltimore, Md., Mono Book Corp., p. 453–474.

Carter, N. L., Christie, J. M., and Griggs, D. T., 1964, Experimen-

tal deformation and recrystallization of quartz: Jour. Geology, v. 72, no. 6, p. 687–733.

Chao, E. C. T., 1967a, Impact metamorphism, *in* Abelson, P. H., ed., Researches in geochemistry, v. 2: New York, John Wiley and Sons, p. 204–233.

——— 1967b, Shock effects in certain rock-forming minerals: Science, v. 156, no. 3772, p. 192–202.

——— 1968, Pressure and temperature histories of impact metamorphosed rocks—based on petrographic observations, *in* French, B. M., and Short, N. M., eds., Shock metamorphism of natural materials: Baltimore, Md., Mono Book Corp., p. 135–158.

Cooper, G. A., and Grant, R. E., 1964, New Permian stratigraphic units in Glass Mountains, west Texas: Am. Assoc. Petroleum Geologists Bull., v. 48, no. 9, p. 1581–1588.

——— 1966, Permian rock units in the Glass Mountains, west Texas: U.S. Geol. Survey Bull., 1244–E, p. E1–E9.

Dachille, Frank, Gigl, Paul, and Simons, P. Y., 1968, Experimental and analytical studies of crystalline damage useful for the recognition of impact structures, *in* French, B. M., and Short, N. M., eds., Shock metamorphism of natural materials: Baltimore, Md., Mono Book Corp., p. 555–569.

Dence, M. R., 1968, Shock zoning at Canadian craters: petrography and structural implications, *in* French, B. M., and Short, N. M., eds., Shock metamorphism of natural materials: Baltimore, Md., Mono Book Corp., p. 169–184.

Dence, M. R., Innes, M. J. S., and Beals, C. S., 1965, On the probable meteorite origin of the Clearwater Lakes, Quebec: Royal Astron. Soc. Canada Jour., v. 59, no. 1, p. 13–22.

Dence, M. R., Innes, M. J. S., and Robertson, P. B., 1968, Recent geological and geophysical studies of Canadian craters, *in* French, B. M., and Short, N. M., eds., Shock metamorphism of natural materials: Baltimore, Md., Mono Book Corp., p. 339–362.

Diehl, C. H. H., and Jones, G. H. S., 1967, The Snowball crater, general background information: Defence Research Establishment (Canada), Suffield Expt. Sta., Tech. Note 187, 23 p.

Dietz, R. S., 1946, Geological structures possibly related to lunar craters: Pop. Astronomy, v. 54, no. 9, p. 465–467.

——— 1960, Meteorite impact suggested by shatter cones in rock: Science, v. 131, no. 3416, p. 1781–1784.

——— 1968, Shatter cones in cryptoexplosion structures, *in* French, B. M., and Short, N. M., eds., Shock metamorphism of natural materials: Baltimore, Md., Mono Book Corp., p. 267–284.

Eggleton, R. E., and Shoemaker, E. M., 1961, Breccia at Sierra Madera, *in* Short papers in the geologic and hydrologic sciences: U.S. Geol. Survey Prof. Paper 424–D, p. D151–D153.

Engel, O. G., 1962, Collisions of liquid drops with liquids, Part II—Crater depth in fluid impacts: U.S. Air Force Systems Command Tech. Rept. WADD–TR–60–475, 52 p.

Engelhart, W. C., Bertsch, W., Stöffler, D., Groschopf, P. and Reiff, W., 1967, Anzeichen für den meteoritschen Ursprung des Beckens von Steinheim: Naturwiss., v. 54, no. 8, p. 198–199.

Engelhart, W. v., and Stöffler, D., 1965, Spaltflächen im Quarz als Anzeichen für Einschläge grosser Meteoriten: Naturwiss., v. 52, no. 17, p. 489–490.

Flawn, P. T., 1956, Basement rocks of Texas and southeast New Mexico: Texas Univ. Pub. 5605, 261 p.

Folk, R. L., 1959, Practical petrographic classification of limestones: Am. Assoc. Petroleum Geologists Bull., v. 43, pt. 1, p. 1–38.

——— 1962, Spectral subdivision of limestone types, *in* Classification of carbonate rocks, a symposium: Am. Assoc. Petroleum Geologists Mem. 1, p. 62–84.

Gault, D. E., Quaide, W. L., and Oberbeck, V. R., 1968, Impact cratering mechanics and structures, *in* French, B. M., and Short, N. M., eds., Shock metamorphism of natural materials: Baltimore, Md., Mono Book Corp., p. 87–99.

Groves, James, 1925, Fossil charophyte fruits from Texas: Am. Jour. Sci., 5th ser., v. 10, no. 1, p. 12–14.

Harlow, F. H., and Shannon, J. P., 1967a, The splash of a liquid drop: Jour. Appl. Physics, v. 38, no. 10, p. 3855–3866.

——— 1967b, Distortion of a splashing liquid drop: Science, v. 157, no. 3788, p. 547–550.

Hörz, Friedrich, 1968, Statistical measurements of deformation structures and refractive indices in experimentally shock loaded quartz, *in* French, B. M., and Short, N. M., eds., Shock metamorphism of natural materials: Baltimore, Md., Mono Book Corp., p. 243–353.

Howard, K. A. and Offield, T. W., 1968, Shatter cones at Sierra Madera, Texas: Science, v. 162, no. 3850, p. 261–265.

Kieffer, S. W., 1969, Shock wave propagation through granular quartz [abs.]: Am. Geophys. Union Trans., v. 50, no. 4, p. 221.

King, P. B., 1930, The geology of the Glass Mountains, Texas, Part 1, Descriptive geology: Texas Univ. Bull. 3038, 167 p.

——— 1942, Permian of west Texas and southeastern New Mexico, Part 2 *of* DeFord, R. K., and Lloyd, E. R., eds., West Texas-New Mexico Symposium: Am. Assoc. Petroleum Geologists Bull., v. 26, no. 4, p. 535–763.

——— 1948, Geology of the southern Guadalupe Mountains, Texas: U.S. Geol. Survey Prof. Paper 215, 183 p.

Lowman, P. D., Jr., 1965, Magnetic reconnaissance of Sierra Madera, Texas, and nearby igneous intrusions, *in* Geological problems in lunar research: New York Acad. Sci. Annals, v. 123, art. 2, p. 1182–1197.

Manton, W. I., 1965, The orientation and origin of shatter cones in the Vredefort ring, *in* Geological problems in lunar research: New York Acad. Sci. Annals, v. 123, art. 2, p. 1017–1049.

Milton, D. J., 1969, Gosses Bluff astrobleme, Australia—shatter cones [abs.]: Am. Geophys. Union Trans., v. 50, no. 4, p. 220.

Milton, D. J., and Brett, Robin, 1968, Gosses Bluff astrobleme, Australia—the central uplift [abs.]: Geol. Soc. America, 64th Ann. Mtg., Tucson, Ariz., Program, p. 82.

Moore, H. J., 1969, Subsurface deformation resulting from missile impact, U.S. Geol. Survey Prof. Paper 650–B, p. B107–B112.

Muehlberger, W. R., 1959, Internal structure of the Grand Saline salt dome, Van Zandt County, Texas: Texas Univ., Bur. Econ. Geology Rept., no. 38, 18 p.

Müller, W. F., and Défourneaux, M., 1968, Deformationsstrukturen in Quarz als Indikator für Stosswellen: Eine experimentelle Untersuchung an Quarz-Einkristallen: Zeitschr. Geophysik, v. 34, no. 5, p. 483–504.

National Research Council's Committee on Stratigraphy, Permian Subcommittee, 1960, Correlation of the Permian formations of North America: Geol. Soc. America Bull., v. 71, no. 12, pt. 1, p. 1763–1805.

Nettleton, L. L., 1955, History of concepts of Gulf Coast salt-dome formation: Am. Assoc. Petrol. Geol. Bull., v. 39, no. 12, p. 2373–2383.

Oriel, S. S., Myers, D. A., and Crosby, E. J., 1967, West Texas Permian basin region, Chap. C, *in* McKee, E. D., Oriel, S. S., and others, Paleotectonic investigations of the Permian System in the United States: U.S. Geol. Survey Prof. Paper 515, p. C19–C60.

Parker, T. J., and McDowell, A. N., 1955, Model studies of salt-dome tectonics: Am. Assoc. Petrol. Geol. Bull., v. 39, no. 12, p. 2384–2470.

Partridge, W. S., and Van Fleet, H. B., 1959, Similarities between lunar and high-velocity-impact craters: Astrophys. Jour., v. 128, p. 416–419.

Rinehart, J. S., 1968, Intense destructive stresses resulting from stress wave interactions, *in* French, B. M., and Short, N. M., eds., Shock metamorphism of natural materials: Baltimore, Md., Mono Book Corp., p. 31–42.

Robertson, P. B., Dence, M. R., and Vos, M. A., 1968, Deformation in rock-forming minerals from Canadian craters, *in* French, B. M., and Short, N. M., eds., Shock metamorphism of natural materials: Baltimore, Md., Mono Book Corp., p. 433–452.

Roddy, D. J., 1968a, The Flynn Creek crater, Tennessee, *in* French, B. M., and Short, N. M., eds., Shock metamorphism of natural materials: Baltimore, Md., Mono Book Corp., p. 291–322.

——— 1968b, Comet impact and formation of Flynn Creek and other craters with central peaks [abs.]: Am. Geophys. Union Trans., v. 49, no. 1, p. 272.

——— 1969a, Shatter cones at TNT explosion craters [abs.]: Am. Geophys. Union Trans., v. 50, no. 4, p. 220.

——— 1969b, Similarities of 100 and 500 ton TNT explosion craters and proposed comet impact craters [abs.]: Am. Geophys. Union Trans., v. 50, no. 4, p. 220.

Rooke, A. D., Jr., and Chew, T. D., 1965, Operation Snowball, Project 3.1—Crater measurements and earth media determinations, interim report: U.S. Army Eng. Waterways Expt. Sta. Misc. Paper I–764, 61 p.

Shoemaker, E. M., 1960, Penetration mechanics of high velocity meteorites, illustrated by Meteor Crater, Arizona: Internat. Geol. Cong., 21st, Copenhagen 1960, Rept., pt. 18, p. 418–434.

——— 1962, Interpretation of lunar craters, *in* Kopal, Zdeněk, ed., Physics and astronomy of the Moon: New York, Academic Press, p. 283–380.

——— 1963, Impact mechanics at Meteor Crater, Arizona, *in* Middlehurst, B. M., and Kuiper, G. P., eds., The moon, meteorites, and comets, v. 4, *of* The solar system: Chicago, Ill., Univ. Chicago Press, p. 301–336.

——— 1968, Structure of the Jangle U and Teapot ESS nuclear explosion craters [abs.], *in* French, B. M., and Short, N. M., eds., Shock metamorphism of natural materials: Baltimore, Md., Mono Book Corp., p. 627–628.

Shoemaker, E. M., and Eggleton, R. E., 1964, Re-examination of the stratigraphy and structure of Sierra Madera, Texas, *in* Astrogeologic Studies Ann. Prog. Rept., Aug. 25, 1962–July 1, 1963: U.S. Geol. Survey open-file rept., pt. B, p. 98–106.

Shoemaker, E. M., Gault, D. E., Moore, H. J., and Lugn, R. V., 1963, Hypervelocity impact of steel into Coconino sandstone: Am. Jour. Sci., v. 261, no. 7, p. 668–682.

Short, N. M., 1965, A comparison of features characteristic of nuclear explosion craters and astroblems, *in* Geological problems in lunar research: New York Acad. Sci. Annals, v. 123, art. 2, p. 573–616.

——— 1966a, Shock processes in geology: Jour. Geol. Education, v. 14, no. 4, p. 149–166.

——— 1966b, Effects of shock pressures from a nuclear explosion on mechanical and optical properties of granodiorite: Jour. Geophys. Research, v. 71, no. 4, p. 1195–1215.

——— 1968a, Experimental microdeformation of rock materials by shock pressures from laboratory-scale impacts and explosions, *in* French, B. M., and Short, N. M., eds., Shock metamorphism of natural materials: Baltimore, Md., Mono Book Corp., p. 219–242.

——— 1968b, Nuclear-explosion-induced microdeformation of rocks: an aid to the recognition of meteorite impact structures, *in* French, B. M., and Short, N. M., eds., Shock metamorphism of natural materials: Baltimore, Md., Mono Book Corp., p. 185–210.

Short, N. M., and Bunch, T. E., 1968, A worldwide inventory of features of rocks associated with presumed meteorite impact craters, *in* French, B. M., and Short, N. M., eds., Shock metamorphism of natural materials: Baltimore, Md., Mono Book Corp., p. 255–266.

Simkin, Thomas, 1967, Flow differentiation in the picritic sills of North Skye, *in* Wyllie, P. J., ed., Ultramafic and related rocks: New York, John Wiley & Sons, p. 64–68.

Snyder, F. G., and Gerdemann, P. E., 1965, Explosive igneous activity along an Illinois-Missouri-Kansas axis: Am. Jour. Sci., v. 263, no. 6, p. 465–493.

Stearns, R. G., Wilson, C. W., Jr., Tiedmann, H. A., Wilcox, J. T., and Marsh, P. S., 1968, The Wells Creek structure, Tennessee, *in* French, B. M., and Short, N. M., eds., Shock metamorphism of natural materials: Baltimore, Md., Mono Book Corp., p. 323–337.

U.S. Geological Survey, 1967, Gosses Bluff structure, *in* Astrogeologic Studies Ann. Prog. Rept., July 1, 1966–Oct. 1, 1967: U.S. Geol. Survey open-file rept., p. 31–35.

Van Lopik, J. R., and Geyer, R. A., 1963, Gravity and magnetic anomalies of the Sierra Madera, Texas "dome": Science, v. 142, no. 3588, p. 45–47.

Vertrees, C. D., Atchison, C. H., and Evans, G. L., 1959, Paleozoic geology of the Delaware and Val Verde basins, *in* Geology of the Val Verde basin and field trip guidebook: West Texas Geol. Soc., p. 64–73.

Williams, Howel, Turner, F. J., and Gilbert, C. M., 1954, Petrography—an introduction to the study of rocks in thin section: San Francisco, Calif., W. H. Freeman and Co., 406 p. (repr. 1958).

Wilshire, H. G., 1961, Layered diatremes near Sydney, New South Wales: Jour. Geology, v. 69, no. 4, p. 473–484.

——— 1969, Mineral layering in the Twin Lakes granodiorite, Colorado, *in* Larsen, E. H., ed., Petrological and structural studies: Geol. Soc. America Mem. 115, Poldervaart Volume, p. 235–261.

Wilshire, H. G., and Howard, K. A., 1968, Structural pattern in central uplifts of cryptoexplosion structures as typified by Sierra Madera: Science, v. 162, no. 3850, p. 258–261.

Wilson, C. W., Jr., and Stearns, R. G., 1969, Lateral and vertical movements of rock in the Wells Creek structure, Tennessee [abs.]: Geol. Soc. America Southeastern Sec., 18th Ann. Mtg., p. 87.

Worthington, A. M., 1963, A study of splashes: New York, Macmillan Co., 169 p.

Young, Addison, 1960, Paleozoic history of the Fort Stockton-Del Rio region, west Texas, *in* Aspects of the geology of Texas—A symposium: Texas Univ. Pub. 6017, p. 87–109.

Zimmermann, R. A., and Amstutz, G. C., 1965, The polygonal ring structure at Decaturville, Missouri: new tectonic observations: Neues Jahrb. Mineralogie Monatsh., v. 9, no. 11, p. 288–307.

U. S. GOVERNMENT PRINTING OFFICE : 1973 O - 477-953